

094044
9

Cerro Toledo Rhyolite, Jemez Volcanic Field, New Mexico: ⁴⁰Ar/³⁹Ar geochronology of eruptions between two caldera-forming events

Terry L. Spell* *Department of Geosciences, University of Houston, Houston, Texas 77204-5503 and
Research School of Earth Sciences, Australian National University, Canberra ACT 0200, Australia*
Ian McDougall *Research School of Earth Sciences, Australian National University, Canberra ACT 0200, Australia*
Anthony P. Doulgeris

ABSTRACT

The Cerro Toledo Rhyolite comprises a group of domes and tephra which were erupted during the interval between two caldera-forming ignimbrites, the Tshirege Member and Otowi Member of the Banderlier Tuff, in the Jemez Volcanic Field, New Mexico. To provide a chronologic framework for geochemical and isotopic studies on these rhyolites, which record the evolution of the Banderlier magma system during this interval, a ⁴⁰Ar/³⁹Ar geochronology study was undertaken. Pumice from major pyroclastic fall deposits within the rhyolite tephra and samples from the rhyolite domes were dated as well as the stratigraphically bracketing Banderlier Tuff. Analyzed crystal populations range from being fairly homogeneous juvenile material to very heterogeneous mixed juvenile and xenocrystic assemblages. In most cases dominant groups of juvenile sanidine crystals define ⁴⁰Ar/³⁹Ar ages which agree with stratigraphic constraints. Plagioclase analyses are distinctly more scattered and do not typically define reasonable ages. The ⁴⁰Ar/³⁹Ar ages for the two members of the Banderlier Tuff yield an interval of 380 ± 20 k.y. between these caldera-forming eruptions. During this interval nine major pyroclastic pumice units were deposited in the sections studied, for which six yield isochron ages, one a weighted mean age, one a maximum age, and one no reliable age due to lack of sanidine. ⁴⁰Ar/³⁹Ar dates on pumice fall units within the Cerro Toledo Rhyolite tephra indicate that eruptive activity occurred at >1.59, 1.54, 1.48, 1.37 and 1.22 Ma. ⁴⁰Ar/³⁹Ar dating of Cerro Toledo Rhyolite domes indicates these were erupted within the caldera at 1.54, 1.45, 1.38–1.34, and 1.27 Ma. The dates

obtained indicate that eruptive activity occurred throughout the 380 k.y. interval between the two members of the Banderlier Tuff, but suggest that eruptions producing both tephra and domes occurred during discrete intervals at ca. 1.54, 1.48, and 1.38–1.34 Ma. The interval from 1.34 to 1.38 Ma was particularly active; 7 of 18 units dated are these ages.

INTRODUCTION

The mechanisms by which silicic magma chambers are generated and evolve continues to be debated (e.g., Smith, 1979; Hildreth, 1981; Lipman, 1984; Huppert and Sparks, 1988; Halliday et al., 1989; Christensen and DePaolo, 1993; Davies et al., 1994; Bogaard, 1995). Eruption triggering events, processes of crystallization within the magma chamber, and the longevity of large upper crustal magma chambers have been intensely studied, but are not well understood. Multicyclic caldera systems in which the products of postcollapse volcanism are preserved provide the potential for studying these processes in detail. Voluminous ignimbrites record the characteristics of the magma chamber at an instant in time, whereas postcollapse volcanism records temporal evolution of the magma system and may yield insights into the transitions to and from these large eruptions and caldera collapse events. Good chronological constraints on, for example, rates of differentiation and timing of recharge events, are essential to the interpretation of geochemical and isotopic data from such systems.

The Valles-Toledo caldera complex, located near the center of the Jemez Volcanic Field (Fig. 1), provides an ideal opportunity for studying the evolution of silicic magma systems associated with multicyclic caldera complexes. This is because the products of two caldera-forming ignimbrite eruptions as well as postcollapse rhyolite domes and tephra are well preserved and exposed. In this study we examine the geochronol-

ogy of the Cerro Toledo Rhyolite, a sequence of small-volume pyroclastic rocks and domes which were erupted during a 380 k.y. interval between two caldera-forming ignimbrites, the Otowi Member Banderlier Tuff (lower stratigraphic unit, ca. 1.61 Ma) and the Tshirege Member Banderlier Tuff (upper stratigraphic unit, ca. 1.23 Ma). These rocks thus record the evolution of the magma system from immediately following one caldera collapse event until immediately prior to the next caldera collapse event. Nine pumice fall units within the Cerro Toledo Rhyolite tephra, nine Cerro Toledo Rhyolite domes, and the bracketing Banderlier tuffs were dated by the single crystal laser fusion ⁴⁰Ar/³⁹Ar technique. These data form an integral part of a preliminary geochemical study (Spell et al., 1996) and will be critical to more detailed future work on the Banderlier silicic magma system.

GEOLOGIC OVERVIEW

The Jemez Volcanic Field is located in north-central New Mexico on the western margin of the Rio Grande rift (Fig. 1). The overall structure of the present-day volcanic field is dominated by basaltic to rhyolitic volcanic rocks of the Polvadera and Keres groups, which form the broad shield upon which younger silicic volcanic rocks of the Tewa Group were erupted (Bailey et al., 1969; Gardner and Goff, 1984; Gardner et al., 1986). Beginning at ca. 1.85 Ma a series of explosive rhyolitic eruptions occurred. The first of these produced the San Diego Canyon ignimbrites, which consist of two small (<10 km²) units (a stratigraphically lower unit A, and an upper unit B) that were vented from a source area beneath the Valles caldera (Self et al., 1986; Turville and Self, 1988; Spell et al., 1990). These were followed by the Banderlier tuffs, which represent ~650 km² of rhyolite magma (Kuentz, 1986; Balsley, 1988). The Otowi Member was erupted 1.608 ± 0.010 Ma and resulted in collapse of the Toledo caldera.



Figure 1. Geologic map of Jemez Volcanic Field showing location of Cerro Toledo rhyolite (CTR) domes and tephra (partly after Smith et al., 1970; Heiken et al., 1986; Stix and Gorton, 1993). Ring fracture post-Valles Caldera domes are shown as unpatterned. Cerro Toledo Rhyolite domes shown by speckled pattern. Major Cerro Toledo Rhyolite tephra outcrops indicated by cross-hatched pattern. Banderlier Tuff is exposed in large outcrop areas to the east and west of the caldera, smaller outcrops are to the north, south, and within the Valles Caldera and Toledo embayment (not shown for clarity). Location of Cerro Toledo Rhyolite tephra sections 6 and 15 in Pueblo Canyon and sample localities for the Banderlier Tuff samples (Kuentz, 1986; Balsley, 1988) are indicated.

whereas the Tshirege Member, or upper Banderlier Tuff (Tshirege Member Banderlier Tuff), was erupted 1.225 ± 0.008 Ma and resulted in formation of the Valles caldera at a nearly coincident location (Smith and Bailey, 1968; Bailey et al., 1969; Heiken et al., 1986; Self et al., 1986). Rhyolite domes and associated tephra, the Cerro Toledo Rhyolite were erupted during the interval between the Otowi Member and the Tshirege Member (Griggs, 1964; Bailey et al., 1969). Preserved Cerro Toledo Rhyolite domes (some were likely destroyed during the collapse of the Valles caldera) are situated in the northeastern half of the Valles caldera and within the Toledo embayment, whereas the tephra are exposed in canyons to the east of the caldera (Fig. 1). Post-collapse rhyolites of the Valles caldera are included in the Valles Rhyolite Formation and consist dominantly of high-silica rhyolite domes and lavas (Griggs, 1964; Bailey et al., 1969; Spell and Kyle, 1989; Spell et al., 1993) which range in age from ca. 1.13 Ma to ca. 50–60 ka (Spell and Harrison, 1993; Reneau et al., 1996).

Previous Geochronology

The first K-Ar geochronology on rhyolites of the Valles caldera complex was reported by Doell and Dabrymple (1966) and the complete dataset was reported by Doell et al. (1968). Their work yielded ages of 1.12 ± 0.03 Ma for the Tshirege Member and 1.45 ± 0.06 Ma for the

Otowi Member (all errors are quoted at the 1 σ level; ages are adjusted, where necessary, to conform with the decay constants and isotopic abundances recommended by Steiger and Jäger, 1977) (Table 1). ⁴⁰Ar/³⁹Ar dating of the Banderlier Tuff and San Diego Canyon ignimbrites was reported by Spell et al. (1990), who obtained ages of 1.14 ± 0.02 Ma (Tshirege Member), 1.51 ± 0.03 Ma (Otowi Member), and 1.78 ± 0.07 and 1.78 ± 0.04 Ma for San Diego Canyon ignimbrites A and B (lower and upper stratigraphic units), respectively. These ages were based on an age of 17.9 Ma for the Bern 4M muscovite standard from the interlaboratory calibration of Dabrymple and Lanphere (1971). In order to directly compare the ⁴⁰Ar/³⁹Ar ages of Spell et al. (1990) with those reported in this study they must be increased by 3.9% because Bern 4M has an age of 18.6 Ma relative to 27.9 Ma for the Fish Canyon Tuff sanidine standard used here (Hurford and Hammerschmidt, 1985). This yields ages of 1.19 ± 0.02 Ma, 1.57 ± 0.03 Ma, and 1.85 ± 0.07 Ma for the Tshirege Member, Otowi Member and San Diego Canyon ignimbrites, respectively. Izzet and Obradovich (1994) reported ⁴⁰Ar/³⁹Ar ages on several Jemez rhyolites including the Tshirege Member and Otowi Member. They obtained weighted mean ages of 1.24 ± 0.02 Ma for the Tshirege Member and 1.63 ± 0.01 Ma for the Otowi Member (adjusted to an age of 27.9 Ma for the Fish Canyon Tuff sanidine standard).

A summary of published chronological data on the Cerro Toledo Rhyolite was given by Stix et al. (1988). Izzet et al. (1981) reported K-Ar ages on a unit of the Cerro Toledo Rhyolite toward the middle of the section and on a unit near the top of the section of 1.47 ± 0.04 Ma and 1.23 ± 0.02 Ma, respectively (Table 1). Izzet et al. also reported zircon fission track ages of 1.39 ± 0.06 and 1.46 ± 0.06 Ma for this sample. Stix et al. (1988) reported a K-Ar age of 1.52 ± 0.04 Ma on a sample from stratigraphic level 27 (Table 1). Additional age data, summarized by Stix et al. (1988), from rhyolite domes of the Cerro Toledo Rhyolite that may provide chronological ties with the tephra are discussed below.

A stratigraphic chronology based on the K-Ar age data from Cerro Toledo Rhyolite tephra is in Table 1. The data suggest that more than half of the Cerro Toledo Rhyolite tephra stratigraphic sequence in the sections studied was erupted ca. 1.5 Ma; the K-Ar age for the Otowi Member and stratigraphic levels 22 and 27 (near the middle of the sequence) are indistinguishable at the 2σ level. An apparent hiatus of ca. 290 k.y. appears between level 22 and the next dated horizon, level 41, which has an age indistinguishable from the K-Ar age of the Tshirege Member.

METHODS AND DATA TREATMENT

Nine Plinian pumice fall units within the Cerro Toledo Rhyolite tephra and nine Cerro

1494

*Present address: Spell, Department of Geosciences, University of Nevada, 4505 Maryland Parkway, Las Vegas, Nevada 89154.

RECEIVED
OCT 24 2006

CERRO TOLEDO RHYOLITE, JEMEZ VOLCANIC FIELD, NEW MEXICO

TABLE 1. STRATIGRAPHIC RELATIONS AND GEOCHRONOLOGY OF CERRO TOLEDO RHYOLITE TEPHRA AND ASSOCIATED UNITS

Stratigraphic level ¹	Section 6'	Section 15'	Sample ID	K/Ar (Ma ± σ)	40Ar/39Ar (Ma ± σ)		
					Isotopion	Mean	Weighted mean
45	—	—	927 (TM)	1.12 ± 0.007 ^a	1.225 ± 0.006 ^b	1.220 ± 0.007	1.212 ± 0.006
44	6-11	—	—	—	—	—	—
43	—	—	—	—	—	—	—
41	6-8	—	CT-9	1.23 ± 0.02 ^a	1.212 ± 0.008 ^b	1.213 ± 0.010	1.212 ± 0.007
38	—	15-6	CT-5	—	1.362 ± 0.018 ^b	1.406 ± 0.024	1.389 ± 0.011
36	—	15-12	CT-5	—	1.378 ± 0.018 ^b	1.387 ± 0.012	1.384 ± 0.008
34	—	15-7	—	—	—	—	—
33	—	15-11	—	—	—	—	—
30	6-8	—	—	—	—	—	—
27	6-9	—	CT-8	1.52 ± 0.04 ^a	1.479 ± 0.020 ^b	1.457 ± 0.016	1.459 ± 0.008
26	6-4	—	—	—	—	—	—
23	6-4	—	—	—	—	—	—
22	6-3	—	CT-7	1.47 ± 0.04 ^a	N.D.O. (a)	1.543 ± 0.096 (b)	1.520 ± 0.018 (c)
					N.D.O. (b)	1.324 ± 0.215 (b)	1.205 ± 0.024 (b)
					N.D.O. (c)	1.474 ± 0.028 (b)	1.484 ± 0.024 (b)
					N.D.O. (d)	1.370 ± 0.142 (b)	1.287 ± 0.019 (b)
21	6-2	—	—	—	—	—	—
18	6-1	15-10	CT-3	—	1.451 ± 0.022	1.531 ± 0.032	1.542 ± 0.008 ^d
15	—	15-5	—	—	—	—	—
14	—	15-9	CT-2	—	1.536 ± 0.018 ^b	1.558 ± 0.033	1.550 ± 0.008
11	—	15-4	—	—	—	—	—
10	—	15-8	—	—	—	—	—
9	—	15-8	—	—	—	—	—
8	—	15-8	CT-1	—	N.D.O.	1.663 ± 0.032	1.652 ± 0.006
7	—	15-8	—	—	—	—	—
6	—	—	—	—	—	—	—
5	—	—	—	—	—	—	—
2	—	—	17-31 (DM)	1.45 ± 0.061 ^a	1.808 ± 0.010 ^b	1.611 ± 0.008	1.609 ± 0.008

¹After Australian National University data. N.D.O. = no data obtained. TM = Tephra Member; Banderlier Tuff; DM = Crown Member; Banderlier Tuff. Isotopion ages calculated using thermal ionization TIM (1969) 18 routine and emitting factors and MSWD ≤ 2.5 , errors include J and MSWD. Weighted mean ages use weighting by the inverse of the variance, errors include 0.5% J factor error. Mean ages are sample mean \pm population standard deviation. Means and weighted means are calculated using model apparent ages and routine analyses (a) to (d) from the mean. All ⁴⁰Ar/³⁹Ar analyses are sensitive unless otherwise indicated. For samples where both sanidine and plagioclase were analyzed, s = sanidine, p = plagioclase.
²Stratigraphic levels and section unit numbers from Dix (1988).
³Dix et al. (1988).
⁴Phanerozoic ages.
⁵Dix et al. (1988).
⁶Dix et al. (1988).

Toledo Rhyolite domes within the Valles-Toledo caldera complex were sampled (Fig. 1, Tables 1 and 2). The pumice-fall samples were collected from two sections (6 and 15), located 1.2 km apart in Pueblo Canyon in order to sample the complete Cerro Toledo Rhyolite stratigraphy between the two members of the Banderlier Tuff and are considered to represent the most significant eruptive events preserved within this sequence (i.e., the onset of an eruption within the caldera). The Cerro Toledo Rhyolite tephra consists of Plinian pumice fall units, phreatomagmatic fall and surge ash beds, and epiclastic sedimentary rocks (Six et al., 1988). The tephra are dominantly phenocryst poor, containing <5% crystals; the major phases are quartz and sanidine, and plagioclase is usually constituting a minor phase (Six et al., 1988). Most units contain separate amounts of sanidine, and this was the primary phase analyzed. For units where sanidine was sparse, both sanidine and plagioclase were analyzed. Dome samples range from nearly aphyric to phenocryst rich (>25%); most have <5%–10% phenocrysts. Cerro Toledo Rhyolite tephra samples were dated at the Australian National University, and dome samples were

dated at the University of Houston. Analytical procedures are discussed separately below. Mineral separates were prepared at the Australian National University. Unaltered pumice clasts (<1 to <5 cm) were wire brushed to remove surface material and then crushed. Approximately 10–30 clasts were used for each separate. Whole-rock samples were crushed and sieved. Sanidine and plagioclase were obtained by standard heavy liquid techniques followed by hand picking, and were ultrasonically treated in dilute HF (7%) for 10 min to remove adhering glass. Separated crystals ranged in size from <0.5 to 2 mm and weighed from <0.5 to 5 mg. Australian National University Laboratory Methods
 Samples analyzed at the Australian National University were wrapped in Sn foil and stacked in a silica tube for irradiation. Samples were alternated with fluence monitors (standard minerals), 92–176 sanidine (separated from the Fish Canyon Tuff), such that <5 mm separated fluence monitor positions. Loaded silica tubes were packed in an Al irradiation container lined with

0.2-mm-thick Cd for shielding against thermal neutrons. Synthetic K-bearing glass (obtained from B. Turris, U.S. Geological Survey) and optical grade CaF₂ were included in the irradiation packages to monitor neutron induced argon interferences from K and Ca. Irradiations (10 h) done in the X33 or X34 positions adjacent to the core of the HFAR nuclear reactor at Lucas Heights, New South Wales. Sample containers were inserted three times during the irradiations in order to reduce neutron fluence gradients in both the horizontal and vertical dimensions. Correction factors determined by repeated isotopic analysis of irradiated K glass and CaF₂ fragments were: (³⁹Ar/³⁹Ar)_K = 2.37 (± 0.19) × 10³ (irradiation can K7981/81) and 1.84 (± 0.26) × 10³ (irradiation can K746/82). (³⁹Ar/³⁹Ar)_{Ca} = 3.50 (± 0.14) × 10⁴ and (³⁹Ar/³⁹Ar)_{Ca} = 7.86 (± 0.01) × 10⁴. J factors were determined by laser fusions of 4–5 single crystals (<0.2 mg) of the Fish Canyon Tuff sanidine standard, which yielded reproducibility of 0.11% to 0.45% (standard deviation of population) at each level, within the range of mass spectrometer analytical errors for individual analyses. An error in J of 0.5% was used in age calculations. Variation in

SPILL ET AL.

TABLE 2. GEOCHRONOLOGY OF CERRO TOLEDO RHYOLITE DOMES AND ASSOCIATED UNITS

Sample ID	Dome	K/Ar (Ma ± σ)	40Ar/39Ar (Ma ± σ)		
			Isotopion	Mean	Weighted mean
WS-2	Warm Springs	1.25 ± 0.04 ^a	1.268 ± 0.011 ^b	1.287 ± 0.025	1.283 ± 0.011
TE-9	Santa Fe Islets	—	1.308 ± 0.018 ^b	1.308 ± 0.027	1.306 ± 0.012
TE-15	Turkey Ridge	1.24 ± 0.03 ^a	1.343 ± 0.015 ^b	1.351 ± 0.026	1.348 ± 0.021
TE-1	Unsettled dome	1.33 ± 0.02 ^a	1.348 ± 0.015 ^b	1.356 ± 0.013	1.357 ± 0.011
TE-26	Cerro Teagueur	1.27 ± 0.02 ^a	1.288 ± 0.012 ^b	1.306 ± 0.048	1.306 ± 0.011
TE-10	Santa Fe Islets	—	1.279 ± 0.012 ^b	1.287 ± 0.030	1.280 ± 0.011
TE-20	Low Pines East	1.47 ± 0.05 ^a	1.448 ± 0.007 ^b	1.481 ± 0.027	1.477 ± 0.008
TE-18	Indian Point	—	1.483 ± 0.011 ^b	1.457 ± 0.018	1.454 ± 0.009
TE-25	Low Pines West	1.50 ± 0.05 ^a	1.540 ± 0.012 ^b	1.548 ± 0.018	1.549 ± 0.018
17-31 BT	Obelisk Member	1.45 ± 0.08 ^a	1.618 ± 0.011 ^b	1.644 ± 0.052	1.625 ± 0.009

¹Notes: University of Houston data. Isotopion ages calculated using thermal ionization TIM (1969) 18 routine and emitting factors and MSWD ≤ 2.5 , errors include J and MSWD. Weighted mean ages use weighting by the inverse of the variance, errors include 0.5% J factor error. Mean ages are sample mean \pm population standard deviation. Means and weighted means are calculated using model apparent ages and routine analyses (a) to (d) from the mean. All ⁴⁰Ar/³⁹Ar analyses are sensitive unless otherwise indicated. For samples where both sanidine and plagioclase were analyzed, s = sanidine, p = plagioclase.
²Six et al. (1988).
³Phanerozoic ages.
⁴Dix et al. (1988).
⁵Dix et al. (1988).

neutron fluence along the 31 mm length of the Si irradiation tubes was <1%. The excellent reproducibility of the single crystal fluence monitor fusions indicates that no significant neutron flux gradients were present within individual packets of crystals.
 Irradiated crystals, together with CaF₂ and K glass fragments, were placed in a Cu sample tray within an ultrahigh vacuum extraction line and fused using a 10 W Ar ion laser. A binocular microscope and a video camera system was used to view samples during fusion. Reactive gases were removed by a 101.1 eV SAES getter prior to being admitted to a VG3000 mass spectrometer by expansion. The relative volumes of the extraction line and mass spectrometer allowed <82% of the gas to be admitted to the mass spectrometer. Peak intensities were measured using a Daly photomultiplier collector system by peak hopping through seven cycles; initial peak heights were determined by linear regression to the time of gas admission. Mass spectrometer discrimination and sensitivity was maximized by repeated analysis of atmospheric argon aliquots (from an on-line air argon pipette system). Measured ⁴⁰Ar/³⁹Ar ratios were 289% ± 0.6 (1σ), and the appropriate discrimination corrections of 1.00458 to 1.00507 (1 AMU) were applied to isotope ratios. The measured sensitivity of the mass spectrometer was 1.25 × 10⁻¹⁷ mol mV⁻¹. Line blanks were checked after each 3–5 analyses; they averaged 2.5 × 10⁻¹⁶ mol for mass 40 and were undetectable at mass 36. Mass spectrometer backgrounds were measured before each analysis and the appropriate corrections made to subsequent data. Discrimination, sensitivity, blanks, and backgrounds were relatively constant over the period of data collection. Final data reduction and age calculations were done using Macintosh-based software (KARDate) written at the Aus-

tralian National University. An age of 27.9 Ma (Steven et al., 1967; Cebula et al., 1986) was used for the Fish Canyon Tuff sanidine fluence monitor in calculating ages for samples.
 University of Houston Laboratory Methods
 Samples analyzed at the University of Houston were wrapped in Al foil and stacked in a 6-mm-inside-diameter Pyrex tube. Individual packets averaged 3 mm thick and fluence monitors (Australian National University 92-176 Fish Canyon Tuff sanidine) were placed approximately every 6 mm along the tube. Loaded silica tubes were packed in an Al irradiation container. Synthetic K-bearing glass (obtained from B. Turris, U.S. Geological Survey) and optical grade CaF₂ were included in the irradiation packages to monitor neutron induced argon interferences from K and Ca. Samples were irradiated for 5 h in the D3 position on the core side (fuel rods on three sides, moderator on the fourth side) of the INWG TRIGA type reactor in the Nuclear Science Center of Texas A&M University. Irradiations are performed in a dry tube device, shielded against thermal neutrons by a 5 mm thick jacket of B₂O₃ powder, which rotates about its axis at a rate of 0.7 rpm to mitigate horizontal flux gradients. Correction factors for interfering neutron reactions on K and Ca were determined by repeated analysis of K glass and CaF₂ fragments. Measured (³⁹Ar/³⁹Ar)_K values were <0.00012, always within 1σ of 0, thus no correction for the ³⁹Ar/³⁹Ar reaction was made. Ca correction factors were (³⁹Ar/³⁹Ar)_{Ca} = 2.75 (± 0.06) × 10⁴ and (³⁹Ar/³⁹Ar)_{Ca} = 6.82 (± 0.34) × 10⁴. J factors were determined by fusion of 3–5 individual crystals of 92-176 sanidine (Fish Canyon Tuff sanidine), which gave reproducibilities of 0.59 to 0.20% (1 σ) at each standard position. Variation in neutron flux along the

80 mm length of the Si irradiation tubes was <0.5%. An error in J of 0.5% was used in age calculations. No significant neutron flux gradients were present within individual packets of crystals, as indicated by the excellent reproducibility of the single crystal fluence monitor fusions.
 Irradiated crystals together with CaF₂ and K glass fragments were placed in a Cu sample tray in an ultrahigh vacuum extraction line and were fused using a 10 W CO₂ laser. Samples were viewed during fusion by a video camera system, and were positioned on a microtarget sample stage. Reactive gases were removed by a 501.1 eV SAES getter prior to being admitted to a MAP 215-50 mass spectrometer by expansion. The relative volumes of the extraction line and mass spectrometer allow <80% of the gas to be admitted to the mass spectrometer. Peak intensities were measured using a Johnson electron multiplier by peak hopping through seven cycles; initial peak heights were determined by linear regression to the time of gas admission. Mass spectrometer discrimination and sensitivity were maximized by repeated analysis of atmospheric argon aliquots from an on-line pipette system. Measured ⁴⁰Ar/³⁹Ar ratios were 292.9 ± 1.7 (1σ); thus discrimination corrections of 1.00085 to 1.00069 (1 AMU) were applied to measured isotope ratios. The sensitivity of the mass spectrometer was 1.6 × 10⁻¹⁷ mol mV⁻¹. Line blanks were checked after each 3 analyses and averaged 1.2 × 10⁻¹⁶ mol for mass 40 and 2.4 × 10⁻¹⁶ mol for mass 36. Discrimination, sensitivity, and blanks were relatively constant over the period of data collection. Computer-automated operation of the sample stage, laser, extraction line, and mass spectrometer as well as final data reduction and age calculations were done using Macintosh-based software written by A. Deino (University of California, Berkeley). An age of 27.9 Ma (Steven et al., 1967; Cebula et al., 1986) was used for the Fish Canyon Tuff sanidine fluence monitor in calculating ages for samples.
 Inter-calibration of the ⁴⁰Ar/³⁹Ar dating laboratories
 Inter-calibration of the Australian National University ⁴⁰Ar/³⁹Ar data with those from the University of Houston was accomplished by analyzing sample 17-31 (Obelisk Member, Banderlier Tuff) at both laboratories. The fluence monitor for samples run in both labs was 92-176, which is 27.9 Ma sanidine from the Fish Canyon Tuff (Steven et al., 1967; Cebula et al., 1986). This identical results were obtained for the age of sample 17-31 (see below) indicates that the two datasets are directly comparable.
 Data Treatment
 A major advantage of dating individual crystals from explosively erupted volcanic rocks is that mixed crystal populations consisting of ju-

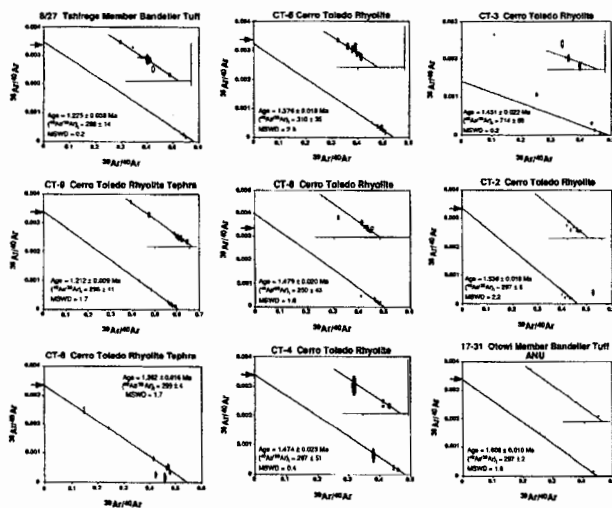


Figure 2 (Above and on following pages). Isochron plots for single crystal $^{40}\text{Ar}/^{39}\text{Ar}$ analyses of the Otowi Member, Tahirege Member, and Cerro Toledo Rhyolite samples. Analyses defining the isochron are shown by solid symbols whereas those omitted are shown by open symbols. Error ellipses are shown at 2σ . Arrows on $^{39}\text{Ar}/^{39}\text{Ar}$ axis indicate composition of atmospheric argon. Note that sample 17-31 (Otowi Member) was analyzed at both the Australian National University (ANU) and the University of Houston (UH).

venile phenocrysts, altered crystals, and xenocrysts can be identified. Ideally this will allow an accurate eruptive age to be calculated based on the ages of juvenile phenocrysts alone, provided that they can be unambiguously identified. Two methods are used here to assess the homogeneity of analyzed crystal populations and to identify juvenile phenocrysts. First, sample means and population standard deviations are calculated. Any samples greater than 2σ from the mean are excluded and a new mean calculated. Weighted means of these refined datasets are also calculated using the inverse of the variance as the weighting factor (Young, 1962). Weighted mean ages are initially calculated using analytical

errors only and a 0.5% J factor error is then incorporated by quadratically combining it with the weighted standard error. Second, isochron ages are calculated using a method outlined previously (Dixon and Pines, 1990; Spell and Harrison, 1993). All analyses are regressed on an isochron using the York (1969) routine. If mean square of weighted deviates (MSWD) is greater than 2.5 (indicating geologic scatter in the data as might be caused by the presence of xenocrysts) the analysis contributing the most to the MSWD is omitted and the remaining data regressed again. This process is repeated if necessary and the result is monitored visually by use of a frequency distribution diagram, until a ho-

monogeneous crystal population is defined. In some cases MSWD falls from above 2.5 to below 1 upon omission of the last outlier. For MSWD less than 1, the standard interpretation is that the analytical errors have been overestimated. In the cases we find here it is most likely the result of having a very homogeneous population of analyses from small crystals, resulting in relatively large errors on each analysis. For samples that define acceptable isochrons, the age and error quoted includes the 0.5% error in J as well as an additional square root of MSWD error to account for scatter in the dataset.

Analyzed crystal populations typically consist of a dominant group of juvenile phenocrysts,

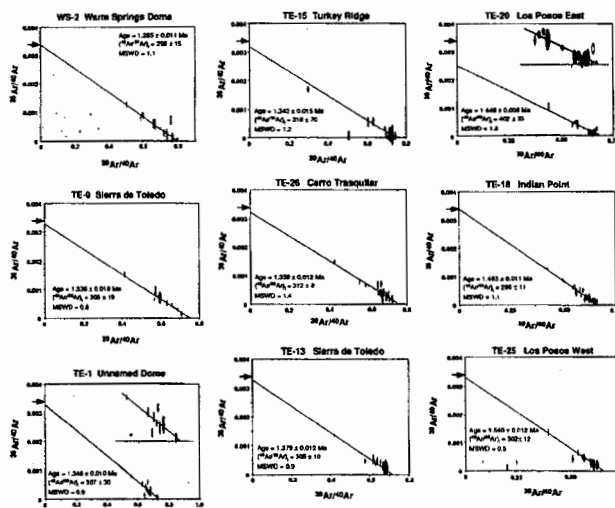


Figure 2. (Continued).

that define the eruptive age, mixed with a lesser number of older (xenocrystic) and younger (altered) crystals, and these outliers are identified and removed from the age calculation by these methods. In a few cases crystal populations are so heterogeneous that age constraints remain ambiguous; this is discussed further.

For most samples a sufficient spread in radiogenic yield among analyses allows reliable isochrons to be defined, and these are taken as giving the preferred age of the unit (see Table 1). For a few samples the weighted mean age is preferred; these are pointed out in the next section. We emphasize that in some cases these methods of calculating an age result in rejection of different analyses; however, the overall agreement in ages by the different methods illustrates the geo-

logical age coherence of the crystal populations and the reliability of the results. Thus, the substitution of ages calculated by the alternate methods for our preferred results does not significantly alter the conclusions of this study.

RESULTS

Cerro Toledo Rhyolite Tephra and Banderler Tuff—Australian National University Data

Eight fusions of sanidine crystals from the Tahirege Member of the Banderler Tuff gave a very homogeneous population of six crystals at ca. 1.22 Ma, and a total range in ages from 1.206 to 1.247 Ma (Table 3). The isochron analysis re-

sults in exclusion of two outliers (samples 827-6a and 827-7a) and yields an age of 1.225 ± 0.008 Ma, an initial $^{40}\text{Ar}/^{39}\text{Ar}$ of 288.3 ± 13.9 , and a mean square of weighted deviates (MSWD) of 0.2 (Figs. 2 and 3, Table 1). The mean and weighted mean analysis results in exclusion of 827-7a and gives similar results of

1.220 ± 0.007 Ma and 1.212 ± 0.006 Ma, respectively (Table 1).

Eight fusions of sanidine crystals from the middle flow unit of the Owoi Member of the Bandler Tuff (sample 17-31) yield apparent ages from 1.580 to 1.623 Ma (Table 3). The isochron approach yields an age of 1.608 ± 0.010 Ma, initial $^{40}\text{Ar}/^{39}\text{Ar}$ of 296.6 ± 2.2, and a MSWD of 1.6 (Figs. 1 and 2) after omitting 1731-5a (Table 1). The mean omits the same analysis and gives an age of 1.611 ± 0.008 Ma and the corresponding weighted mean is 1.609 ± 0.008 Ma (Table 1). These three ages are indistinguishably emphasizing the homogeneous ages of the analyzed crystal population.

Sample 92-CC-01 is from the Owoi Member ignimbrite exposed in a complexly channelled outcrop in Cochiti Canyon (J. A. Wolff, 1994, personal communication). A population of eight analyzed sanidine crystals is heterogeneous, having apparent ages of 1.566 to 1.690 Ma (Table 3). An isochron regression using all the data yields an age of 1.604 ± 0.049 Ma with a MSWD of 35.6. Exclusion of three outliers (Fig. 3) results in an isochron age of 1.601 ± 0.014 Ma, initial $^{40}\text{Ar}/^{39}\text{Ar}$ of 296.7 ± 2.2, and an acceptable MSWD of 2.6 (not shown). The mean age is 1.620 ± 0.042 Ma with no excluded data and the weighted mean is 1.601 ± 0.014 Ma. These ages are indistinguishable from that of the Owoi Member middle flow unit (see above).

Sample CT-9 yielded a very homogeneous population of sanidine apparent ages averaging 1.21 Ma (Fig. 3, Table 3). The 10 analyses fall on an isochron that defines an age of 1.212 ± 0.009 Ma, an initial $^{40}\text{Ar}/^{39}\text{Ar}$ of 295.5 ± 10.6, and a MSWD of 1.7 (Fig. 2). The mean and weighted mean ages of 1.213 ± 0.010 Ma and 1.212 ± 0.007 Ma, respectively, are virtually identical (Table 1) and also include all analyses.

Nine sanidine crystals from sample CT-6 define a dominant group at 1.37 Ma (Table 3). The isochron treatment results in omitting two distinctly older outliers (CT-6-2a and CT-6-7a) and one younger outlier (CT-6-6a). This gives a six-point isochron and an age of 1.362 ± 0.016 Ma, an initial $^{40}\text{Ar}/^{39}\text{Ar}$ of 298.8 ± 3.8, and a MSWD of 1.7 (Figs. 2 and 3). No omissions are indicated for the mean age of 1.404 ± 0.124 Ma, and the corresponding weighted mean is 1.389 ± 0.011 Ma (Table 1). These three age estimates overlap at the 1 σ level.

Ten fusions of sanidine crystals from CT-5 yielded a fairly homogeneous population with a mean of 1.38 Ma (Tables 1 and 3). An isochron regression using all the data yields an age of 1.376 ± 0.018 Ma, an initial $^{40}\text{Ar}/^{39}\text{Ar}$ of 310.6 ± 35.1, and a MSWD of 2.6 (Figs. 2 and 3). Although slightly above the 2.5 MSWD cutoff level, this result is deemed acceptable because the MSWD for the standard isochron ($^{39}\text{Ar}/^{39}\text{Ar}$

vs. $^{40}\text{Ar}/^{39}\text{Ar}$) is 1.7. The mean age indicates exclusion of sample CT-5-5a and gives an age of 1.387 ± 0.012 Ma. The weighted mean of these data is 1.384 ± 0.008 Ma (Table 1). These three estimates of the age are virtually identical and emphasize the age coherence of the analyses.

Ten fusions of sanidine crystals from CT-8 yielded a population at 1.46 Ma (Table 3). The isochron analysis results in omission of one older (CT-8-1a) and one younger outlier (CT-8-9a); the remaining 8 analyses define an isochron age of 1.479 ± 0.020 Ma, an initial $^{40}\text{Ar}/^{39}\text{Ar}$ of 250.9 ± 42.5, and a MSWD of 1.6 (Figs. 2 and 3). The mean indicates that only CT-8-1a be omitted and gives an age of 1.457 ± 0.016 Ma. The weighted mean equivalent is 1.459 ± 0.008 Ma (Table 1). Once again, these age estimates all overlap at the 1 σ level.

Sample CT-7 is nearly aphyric and contains dominantly plagioclase feldspar, and thus both sanidine and plagioclase were analyzed. A total of 13 fusions yielded only two sanidines; the remaining analyses were of plagioclase (identified by CaK α) (Table 3). None of these data define meaningful isochrons. The two sanidine analyses have a mean of 1.543 ± 0.066 Ma and a weighted mean of 1.520 ± 0.016 Ma, whereas the same treatment for the plagioclase analyses omits CT-7-4a and yields a mean of 1.324 ± 0.016 Ma and weighted mean of 1.205 ± 0.024 Ma (Table 1). The two sanidine analyses are broadly consistent with stratigraphic relationships among other Cerro Toledo samples ages; however, the plagioclase ages are either too imprecise or too inconsistent with stratigraphic relationships to be of use in constraining ages. Sample CT-4 is also nearly aphyric; the dominant feldspar is plagioclase, and both sanidine and plagioclase crystals were analyzed. The 6 sanidine analyses define a relatively coherent group at ca. 1.49 Ma, whereas the 10 plagioclase analyses are significantly more heterogeneous and tend to define younger ages, although there are some older ages. A sanidine isochron yields an age of 1.474 ± 0.023 Ma, an initial $^{40}\text{Ar}/^{39}\text{Ar}$ of 296.6 ± 51.4, and a MSWD of 0.4 after omitting analysis CT-4-3a (Figs. 2 and 3). The 6 sanidine analyses define a mean of 1.488 ± 0.024 Ma and a weighted mean of 1.491 ± 0.009 Ma (Table 1). These ages are consistent with stratigraphic relationships. The plagioclase analyses do not define an isochron. A plagioclase mean of 1.370 ± 0.143 Ma and weighted mean of 1.267 ± 0.019 Ma include all 10 plagioclase analyses. As for CT-7, these ages are stratigraphically inconsistent or too imprecise to be useful.

Nine fusions from sample CT-3 yielded apparent ages from 1.474 to 1.998 Ma (Table 3). The isochron procedure results in omitting three of these, a resulting isochron is defined by six analyses (present as two distinct clusters) having a very

narrow range of radiogenic yields (94%–97%), which give an age of 1.431 ± 0.022 Ma, with an apparent initial $^{40}\text{Ar}/^{39}\text{Ar}$ of 714 ± 86 and a MSWD of 2.2. The mean age omits sample CT-3-8a and yields 1.531 ± 0.032 Ma. The weighted mean of these data is 1.542 ± 0.008 Ma (Table 1). Because of the narrow range in radiogenic yield of the CT-3 analyses and the resulting unconstrained isochron, we take the weighted mean as the best estimate of the age of the unit (Table 1).

Sample CT-2 yielded apparent ages for 12 analyses that range from 1.200 to 1.624 Ma (Table 3). Seven of these define an isochron (omitting CT-2-3a, CT-2-4a, CT-2-5a, CT-2-12a, and CT-2-13a) giving an age of 1.536 ± 0.018 Ma with an initial $^{40}\text{Ar}/^{39}\text{Ar}$ of 297.6 ± 8.1 and a MSWD of 2.2 (Figs. 2 and 3). The mean omits only CT-2-12a and gives an age of 1.558 ± 0.033 Ma. The corresponding weighted mean is 1.550 ± 0.008 Ma (Table 1). These three ages are identical at the 1 σ level.

We did 13 fusions on sample CT-1, which is from a rhyolite bed stratigraphically a few metres above the Owoi Member. These yield scattered apparent ages of 1.593 to 1.956 Ma (Table 3), with only the youngest being consistent with its stratigraphic position above the underlying Owoi Member (Fig. 4). These data fail to define an acceptable isochron regardless of how many outliers are omitted. A mean age of 1.653 ± 0.032 Ma omits CT-1-7a and the corresponding weighted mean age is 1.652 ± 0.008 Ma (Table 1). Although the mean age is in agreement with the age of the Owoi Member (see below), these data add no useful constraints to the age of sample CT-1. However, its age is stratigraphically constrained to be between that of the Owoi Member and the overlying CT-2 (Table 1).

Cerro Toledo Rhyolite Domes and Owoi Member—University of Houston Data

Sanidine crystals ($n = 23$) from the Warm Springs dome (WS-3) exhibit the widest range in $^{40}\text{Ar}/^{39}\text{Ar}$ ages from 1.044 to 10.80 Ma (Table 3) of all samples in this study. The isochron approach excludes 10 of these analyses, most significantly older than the mode at 1.152 Ma (Fig. 3) (WS-3g–WS-3o), and one younger crystal (WS-2c), and gives an age of 1.265 ± 0.011 Ma, an atmospheric initial $^{40}\text{Ar}/^{39}\text{Ar}$ of 296 ± 15, with a MSWD of 1.1 (Fig. 2, Table 2). Analyses defining the isochron exhibit a Gaussian distribution with a mode at 1.252 Ma (Fig. 3). When including all analyses, the mean and standard deviations (6.4 ± 20.2 Ma) suggest exclusion of WS-2m only, and thus fail to identify the obvious mode of analyses at 1.252 Ma (Fig. 3). The mean and weighted mean ages of 1.267 ± 0.025 Ma and

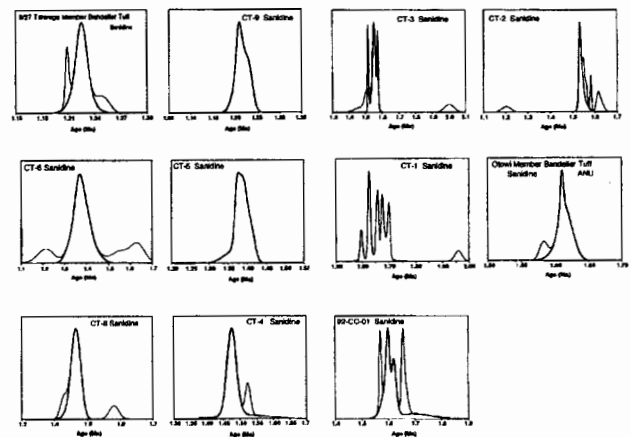


Figure 3 (Above and on facing page). Probability distribution diagrams for the data presented in Figure 2. Thicker curved lines are data used to define isochrons whereas thinner lines show all analyses from a particular unit. Note that sample 17-31 (Owoi Member) was analyzed at both the Australian National University (ANU) and the University of Houston (UoH).

1.263 ± 0.011 Ma, respectively, shown in Table 2 are calculated using the juvenile crystal population defined by the isochron approach and are indistinguishable from the isochron age.

Sample TE-9 from the Sierra de Toledo dome gave a very homogeneous population of sanidine analyses; all 10 fell on an isochron defining an age of 1.336 ± 0.018 Ma, an initial $^{40}\text{Ar}/^{39}\text{Ar}$ of 305 ± 19 and a MSWD of 0.8 (Fig. 2, Table 2). These analyses, after omitting TE-9c, give mean and weighted mean ages of 1.326 ± 0.027 Ma and 1.336 ± 0.012 Ma, respectively, which are indistinguishable from the isochron age.

Fusions of sanidine phenocrysts ($n = 13$) from sample TE-15 from the Turkey Ridge dome yield $^{40}\text{Ar}/^{39}\text{Ar}$ ages ranging from 1.318 to 1.927 Ma, 11 of these forming a coherent group that defines a mode at 1.343 Ma on the probability distribution plot (Fig. 3, Table 3). The isochron approach omits crystals TE-15b and TE-15c (Table 3), which have distinctly older ages than the remaining 11, and gives an age of 1.343 ± 0.015 Ma, an initial

$^{40}\text{Ar}/^{39}\text{Ar}$ of 315 ± 70 and a MSWD of 1.2 (Fig. 2, Table 2). The mean and standard deviation omits analysis TE-15j (1.927 Ma), giving an age of 1.351 ± 0.026 Ma, with the corresponding weighted mean at 1.348 ± 0.021 Ma (Table 2).

Ten sanidine analyses from sample TE-1 from Unmanned dome, range in age from 1.234 Ma to 1.481 Ma, with eight clustered tightly at 1.354 Ma (Fig. 3, Table 3). The isochron approach omits TE-1d and TE-1g, which are older and younger, respectively, than the remaining analyses (Table 3). The isochron defines an age of 1.348 ± 0.010 Ma, with an initial $^{40}\text{Ar}/^{39}\text{Ar}$ of 307 ± 30 and a MSWD of 0.9 (Fig. 2). The mean and weighted means result from omission of the same analyses and are 1.356 ± 0.013 Ma and 1.357 ± 0.011 Ma, respectively.

A total of 21 sanidine fusions from sample TE-26 (Cerro Trinquital) define a fairly homogeneous population. $^{40}\text{Ar}/^{39}\text{Ar}$ ages range from 1.224 Ma to 1.460 Ma, and 17 of these are in the

range 1.321 to 1.416 Ma, giving a mode at 1.378 Ma (Fig. 3, Table 3). The isochron (Fig. 2) is defined by these 17 analyses (TE-26f, TE-26g, and TE-26h omitted), which give an age of 1.359 ± 0.012 Ma, an initial $^{40}\text{Ar}/^{39}\text{Ar}$ of 310 ± 8, and a MSWD of 1.4 (Fig. 2, Table 2). The mean age approach omits only analysis TE-26g and gives an age of 1.368 ± 0.048 Ma with a corresponding weighted mean of 1.369 ± 0.011 Ma (Table 3).

A homogeneous population of $^{40}\text{Ar}/^{39}\text{Ar}$ ages was obtained from fusion of 21 sanidine phenocrysts from sample TE-13 (Sierra de Toledo). The isochron approach includes all analyses and gives an age of 1.379 ± 0.012 Ma, with an initial $^{40}\text{Ar}/^{39}\text{Ar}$ of 305 ± 10 and a MSWD of 0.9 (Fig. 2). The mean age omits analysis TE-13g, giving an age of 1.367 ± 0.030 Ma, and the weighted mean of these analyses is 1.380 ± 0.011 Ma (Table 2).

Sanidine fusions ($n = 22$) from TE-20, Los Pozos East dome, gave a fairly homogeneous

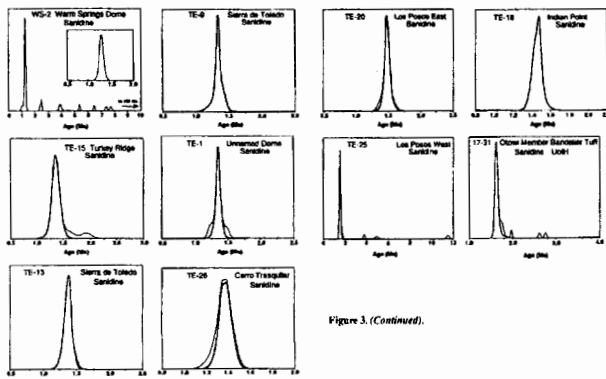


Figure 3. (Continued).

population defining a mode at 1.468 on the probability distribution plot (Fig. 3, Table 3). An acceptable isochron is defined after omitting TE-20v and TE-20u, giving an age of 1.446 ± 0.009 Ma, with a high initial ⁴⁰Ar/³⁹Ar of 402 ± 33, and a MSWD of 1.8 (Fig. 2). The mean age is 1.481 ± 0.027 Ma after omitting TE-20u and TE-20v, and the weighted mean age is 1.477 ± 0.009 Ma (Table 2).

Sandstone crystals (n = 25) were analyzed from sample TE-18, from the Indian Point dike (Table 3). These ages from a Gaussian distribution with a mode at 1.472 Ma (Fig. 3) and a range from 1.386 Ma to 1.533 Ma (Table 3). The isochron analysis includes all the data and gives an age of 1.463 ± 0.011 Ma, with an initial ⁴⁰Ar/³⁹Ar of 296 ± 11, and a MSWD of 1.1 (Fig. 2). The mean omnia analyses TE-18c and TE-18f (older and younger than the mean, respectively) and gives an age of 1.457 ± 0.018 Ma. The corresponding weighted mean age is 1.464 ± 0.009 Ma (Table 2). All of these ages are virtually indistinguishable.

Sandstone analyses (n = 17) from sample TE-25 (Los Posos West) show a strong mode at 1.537 Ma (defined by 13 analyses) with four distinctly older outliers ranging up to 11.51 Ma (Fig. 3, Table 3). The isochron approach results in

omission of these four older analyses and gives an age of 1.540 ± 0.012 Ma, with an initial ⁴⁰Ar/³⁹Ar of 302 ± 12, and a MSWD of 0.5 (Fig. 2). The mean and weighted mean ages of 1.548 ± 0.018 Ma and 1.545 ± 0.016 Ma, respectively, result from omitting the same outliers (Table 2).

Sandstone phenocrysts from sample TE-31 (Owens Member) define ⁴⁰Ar/³⁹Ar ages ranging from 1.583 to 9.459 Ma (Table 3). Isochron analysis shows that after omitting 5 of 33 analyses (17-31f, 17-31i, 17-31j, 17-31k, 17-31l, 17-31m) were excluded, an age of 1.618 ± 0.011 Ma is defined with a trapped ⁴⁰Ar/³⁹Ar of 301 ± 3 and a MSWD of 2.1. The 28 analyses defining the isochron form a coherent group with a mode at 1.62 Ma (Fig. 3). The corresponding mean and weighted mean ages of 1.644 ± 0.033 Ma and 1.625 ± 0.009 Ma result from omitting the same outliers as the isochron.

DISCUSSION

Randell Tuff

The ⁴⁰Ar/³⁹Ar ages obtained in this study of 1.223 ± 0.008 Ma (Australian National University), 1.608 ± 0.010 Ma (Australian National

University) and 1.618 ± 0.011 Ma (University of Houston) for the Tshirege Member and Owens Member, respectively, are 9.4% older (Tshirege Member) to 11.6% older (Owens Member) than the K-Ar dates reported by Doell et al. (1968). This difference is most likely the result of incomplete degassing of sanidine during the K-Ar analyses (e.g., Webb and McDougall, 1967; McDowell, 1983). Spell et al. (1990) obtained ages of 1.19 ± 0.02 Ma and 1.57 ± 0.03 Ma for the Tshirege Member and Owens Member, respectively (when adjusted to an age of 2.9 Ma for the Flat Canyon Tuff; see previous discussion). Izett and Ohtsurovich (1994) reported ages of 1.24 ± 0.02 Ma for the Tshirege Member and 1.63 ± 0.01 Ma for the Owens Member that agree with the ages reported here and are slightly older than (although overlapping at 2σ errors) the ages reported in Spell et al. (1990).

Note that analyses of the Owens Member sample from Cochiti Canyon (92-C-C-01, from a complexly channelled outcrop) form a much more age heterogeneous group than those from sample TE-31 from the massive middle flow unit of the Owens Member. Furthermore the much larger number of analyses of TE-31 at the University of Houston (n = 33) show the presence of xenocrysts which were not apparent from the

TABLE 3. ⁴⁰Ar/³⁹Ar ANALYTICAL DATA FOR CERRO TOLEDO RHYOLITE SAMPLES

Sample ID	⁴⁰ Ar/ ³⁹ Ar (x 10 ³)	Age (Ma)	⁴⁰ Ar/ ³⁹ Ar (x 10 ³)	Age (Ma)	⁴⁰ Ar/ ³⁹ Ar (x 10 ³)	Age (Ma)	⁴⁰ Ar/ ³⁹ Ar (x 10 ³)	Age (Ma)	⁴⁰ Ar/ ³⁹ Ar (x 10 ³)	Age (Ma)	
Tshirege Member, Randell Tuff, Pliocene Unit, J = 0.00029730, Australian National University											
827-1a	6.127	11.78	13.19	24.65	61.3	1.96	1.6997	1.218 ± 0.010			
827-2a	6.264	8.545	9.788	10.56	80.3	1.85	1.7123	1.221 ± 0.012			
827-3a	10.72	10.25	11.51	23.04	85.0	1.96	1.7023	1.220 ± 0.009			
827-4a	6.788	14.12	15.14	28.22	91.5	2.05	1.7068	1.223 ± 0.008			
827-5a	3.153	7.885	8.468	12.12	91.0	2.01	1.7047	1.221 ± 0.014			
827-6a	10.30	12.49	13.13	25.47	88.8	2.06	1.6832	1.204 ± 0.006			
827-7a	2.275	8.402	8.510	15.71	84.2	2.18	1.7403	1.247 ± 0.010			
827-8a	1.230	7.502	8.396	14.92	95.2	1.97	1.7088	1.224 ± 0.008			
Cerro Toledo Rhyolite Tephra, Stratigraphic Level 41, ANU 92-141, J = 0.00049864, Australian National University											
CT8-1a	2.063	6.363	6.841	11.58	93.7	2.11	1.6325	1.205 ± 0.009			
CT8-2a	21.41	8.881	9.127	21.45	86.6	2.14	1.6286	1.210 ± 0.014			
CT8-3a	3.164	6.682	7.128	12.86	91.8	2.26	1.6534	1.221 ± 0.012			
CT8-4a	3.027	6.556	6.728	12.29	89.8	1.89	1.6290	1.208 ± 0.006			
CT8-5a	2.111	4.831	5.283	9.413	92.4	2.05	1.6527	1.219 ± 0.015			
CT8-6a	1.482	2.992	3.225	6.555	94.3	1.97	1.6568	1.222 ± 0.011			
CT8-7a	7.763	6.289	5.220	10.99	78.2	2.84	1.6414	1.211 ± 0.016			
CT8-8a	1.771	7.013	4.563	8.041	92.5	2.38	1.6305	1.203 ± 0.013			
CT8-9a	1.226	6.408	5.225	8.660	92.0	2.28	1.6264	1.203 ± 0.013			
CT8-10a	1.809	5.380	4.828	8.786	93.8	2.27	1.6687	1.231 ± 0.010			
Cerro Toledo Rhyolite Tephra, Stratigraphic Level 38, ANU 92-136, J = 0.00041290, Australian National University											
CT8-1a	78.31	9.212	4.880	26.55	28.7	4.14	1.6665	1.422 ± 0.024			
CT8-2a	2.729	4.107	2.560	5.541	84.7	3.52	1.6264	1.380 ± 0.022			
CT8-3a	1.389	3.781	1.876	3.981	83.0	4.43	1.6800	1.400 ± 0.020			
CT8-4a	1.154	3.487	1.968	4.468	81.6	4.11	1.7102	1.521 ± 0.021			
CT8-5a	4.145	4.880	2.114	5.124	75.4	5.08	1.6296	1.382 ± 0.021			
CT8-6a	0.508	4.322	1.741	3.898	84.4	5.46	2.0440	1.522 ± 0.045			
CT8-8a	15.99	2.234	0.938	6.283	24.3	2.24	1.6251	1.210 ± 0.037			
CT8-9a	1.755	3.904	1.519	3.250	83.3	5.65	1.7824	1.327 ± 0.028			
CT8-10a	10.29	4.118	1.260	5.644	44.8	8.71	1.8295	1.375 ± 0.021			
Cerro Toledo Rhyolite Tephra, Stratigraphic Level 25, ANU 92-137, J = 0.00041414, Australian National University											
CT8-1a	0.558	9.371	4.841	9.970	90.1	4.35	1.6567	1.387 ± 0.011			
CT8-2a	1.874	11.78	7.843	15.53	95.4	3.31	1.6891	1.411 ± 0.011			
CT8-3a	3.548	8.461	4.526	8.975	88.9	3.12	1.6548	1.385 ± 0.016			
CT8-4a	1.389	5.509	3.740	7.414	93.8	3.24	1.6552	1.388 ± 0.015			
CT8-5a	1.872	4.145	3.778	5.640	88.9	3.28	1.6048	1.349 ± 0.022			
CT8-6a	2.149	6.875	3.312	6.877	89.9	4.43	1.6334	1.384 ± 0.019			
CT8-7a	1.263	8.834	3.893	7.448	92.5	5.28	1.6054	1.303 ± 0.014			
CT8-8a	3.383	7.030	3.113	6.845	84.8	4.97	1.6837	1.382 ± 0.011			
CT8-9a	3.123	8.282	4.474	10.58	92.0	3.15	1.6405	1.375 ± 0.016			
CT8-10a	2.193	9.809	4.972	8.649	92.9	4.34	1.6247	1.370 ± 0.020			
Cerro Toledo Rhyolite Tephra, Stratigraphic Level 27, ANU 92-140, J = 0.00049008, Australian National University											
CT8-1a	3.487	8.208	3.220	7.788	96.1	3.44	2.0198	1.498 ± 0.018			
CT8-2a	1.880	20.75	0.379	1.117	51.5	12.00	1.6184	1.124 ± 0.139			
CT8-3a	1.658	14.49	0.250	0.911	47.4	12.8	1.7294	1.281 ± 0.179			
CT8-4a	0.588	17.38	0.315	1.082	84.2	12.1	2.2912	2.068 ± 0.149			
CT8-5a	1.798	21.39	0.338	1.987	80.0	14.1	2.3078	1.709 ± 0.103			
CT8-6a	0.798	21.43	0.382	0.949	76.8	12.4	1.9068	1.413 ± 0.084			
CT8-7a	0.572	14.73	0.291	0.745	78.8	11.2	2.0147	1.482 ± 0.152			
CT8-8a	0.809	10.27	0.281	0.228	87.8	10.0	1.8078	1.413 ± 0.118			
CT8-9a	1.457	4.995	1.687	3.886	87.6	7.34	2.1489	1.590 ± 0.027			
CT8-10a	2.088	17.01	0.317	1.098	44.0	11.8	1.5070	1.153 ± 0.059			
CT7-11a	1.185	11.63	0.187	0.853	47.8	16.3	1.9948	1.471 ± 0.182			
CT7-12a	1.318	15.48	0.251	0.714	47.1	13.6	1.9418	0.984 ± 0.081			
CT7-13a	1.501	21.45	0.445	1.129	82.3	10.6	1.5941	1.180 ± 0.041			
Cerro Toledo Rhyolite Tephra, Stratigraphic Level 21-22, ANU 92-139, J = 0.00049560, Australian National University											
CT4-1a	1.175	8.270	2.916	6.485	93.8	8.0	2.0740	1.485 ± 0.013			
CT4-2a	1.888	31.42	0.823	1.834	73.5	11.1	1.8881	1.320 ± 0.045			
CT4-3a	1.549	18.73	3.865	8.306	93.8	10.0	2.1321	1.521 ± 0.013			
CT4-4a	0.780	17.15	0.547	0.976	78.8	10.9	2.1544	1.838 ± 0.150			
CT4-5a	1.186	30.49	0.815	1.881	88.5	10.9	2.2148	1.580 ± 0.070			
CT4-6a	1.202	6.728	3.082	6.644	93.6	9.3	2.0717	1.478 ± 0.017			

(Continued)

Cerro Toledo Rhyolite, Jemez Volcanic Field, New Mexico

TABLE 3. (Continued)

Sample ID	$^{87}\text{Sr}/^{86}\text{Sr}$	$^{87}\text{Rb}/^{86}\text{Sr}$	Age (Ma ± 1σ)						
	($\pm 1\sigma$)								
Cerro Toledo Rhyolite, Cerro Tresquebra, $J = 0.0005334$, University of Houston (continued)									
TE-26c	0.864	2.294	1.961	2.996	91.7	2.09	1.439	1.366 ± 0.028	
TE-26d	0.868	2.373	1.922	1.946	97.5	4.16	1.369	1.321 ± 0.049	
TE-26e	1.222	1.847	1.101	1.750	79.6	3.00	1.272	1.224 ± 0.055	
TE-26f	1.088	1.556	0.980	1.618	80.5	2.85	1.316	1.271 ± 0.059	
TE-26g	1.227	0.000	2.037	3.087	68.3	0.00	1.324	1.287 ± 0.037	
TE-26h	2.672	0.356	1.849	3.923	78.0	0.36	1.484	1.437 ± 0.040	
TE-26i	0.868	0.901	1.368	2.197	86.1	0.00	1.432	1.372 ± 0.049	
Cerro Toledo Rhyolite, Sierra de Toledo, $J = 0.0009478$, University of Houston									
TE-13a	2.032	4.197	2.867	4.524	86.9	2.55	1.379	1.311 ± 0.044	
TE-13b	0.432	4.203	3.109	4.612	97.3	2.43	1.446	1.430 ± 0.050	
TE-13c	0.578	2.122	1.417	2.092	92.1	2.99	1.359	1.340 ± 0.113	
TE-13d	0.880	9.887	6.456	10.305	86.2	2.70	1.373	1.362 ± 0.027	
TE-13e	0.832	2.928	2.189	3.185	92.5	2.41	1.349	1.320 ± 0.069	
TE-13f	0.418	2.011	2.132	3.129	92.2	1.70	1.383	1.381 ± 0.038	
TE-13g	1.680	2.812	1.883	3.424	85.9	2.54	1.446	1.475 ± 0.028	
TE-13h	4.468	4.222	2.822	6.710	56.4	2.60	1.400	1.403 ± 0.031	
TE-13i	0.192	1.211	0.800	1.389	95.1	2.33	1.421	1.404 ± 0.070	
TE-13j	0.460	1.384	0.868	1.291	91.1	2.81	1.362	1.349 ± 0.072	
TE-13k	0.848	1.728	1.808	2.897	90.9	1.72	1.395	1.342 ± 0.036	
TE-13l	1.504	2.021	2.108	3.288	87.0	1.72	1.364	1.378 ± 0.031	
TE-13m	0.352	1.278	1.442	2.092	95.2	1.58	1.384	1.387 ± 0.046	
TE-13n	0.976	5.786	3.768	5.830	95.0	2.74	1.429	1.406 ± 0.018	
TE-13o	0.528	1.172	1.255	1.888	91.9	1.87	1.371	1.364 ± 0.054	
TE-13p	0.338	1.334	1.250	1.840	94.8	1.91	1.379	1.380 ± 0.052	
TE-13q	0.960	1.708	2.873	3.544	97.0	0.59	1.411	1.396 ± 0.020	
TE-13r	0.992	2.097	1.122	1.820	84.2	3.34	1.368	1.351 ± 0.085	
TE-13s	0.688	2.744	2.129	3.115	93.8	2.29	1.358	1.349 ± 0.026	
TE-13t	0.240	0.901	0.754	1.118	93.9	0.00	1.394	1.373 ± 0.069	
TE-13u	0.960	2.302	1.298	1.982	88.0	3.29	1.349	1.332 ± 0.068	
Cerro Toledo Rhyolite, Los Peñas East, $J = 0.0009478$, University of Houston									
TE-20a	0.224	6.412	3.671	5.972	96.9	3.15	1.521	1.503 ± 0.040	
TE-20b	0.548	6.878	4.973	7.592	99.9	2.42	1.472	1.461 ± 0.020	
TE-20c	0.016	5.348	3.489	5.048	100.0	2.78	1.454	1.431 ± 0.048	
TE-20d	0.380	20.510	14.603	21.812	99.7	2.53	1.481	1.463 ± 0.012	
TE-20e	0.416	3.322	2.445	3.996	96.8	2.45	1.467	1.439 ± 0.081	
TE-20f	1.284	2.917	1.815	3.299	98.9	2.18	1.524	1.504 ± 0.064	
TE-20g	0.352	2.456	2.079	3.148	98.8	2.12	1.471	1.444 ± 0.034	
TE-20h	2.528	4.476	3.083	5.400	88.5	2.63	1.536	1.507 ± 0.029	
TE-20i	0.304	1.844	1.638	2.375	99.5	2.13	1.529	1.498 ± 0.049	
TE-20j	0.018	2.807	1.842	2.954	99.9	2.09	1.526	1.498 ± 0.037	
TE-20k	2.844	6.050	3.215	5.603	85.3	2.81	1.498	1.465 ± 0.030	
TE-20l	0.180	1.778	1.197	1.828	97.5	2.87	1.491	1.463 ± 0.050	
TE-20m	1.840	1.354	0.752	1.701	88.5	3.25	1.520	1.502 ± 0.082	
TE-20n	0.320	5.627	2.629	4.221	97.9	3.58	1.492	1.471 ± 0.022	
TE-20o	0.480	4.438	2.289	3.556	98.2	3.47	1.496	1.470 ± 0.032	
TE-20p	1.200	5.432	2.809	4.787	92.7	3.31	1.521	1.494 ± 0.024	
TE-20q	0.918	10.790	4.515	7.110	95.1	4.30	1.512	1.488 ± 0.018	
TE-20r	0.128	12.329	3.741	5.800	99.5	5.92	1.547	1.519 ± 0.027	
TE-20s	0.180	7.433	2.031	3.090	98.7	6.57	1.504	1.478 ± 0.026	
TE-20t	0.224	8.199	1.468	2.337	97.5	8.63	1.530	1.508 ± 0.048	
TE-20u	0.856	1.850	1.908	2.840	93.3	1.15	1.391	1.365 ± 0.047	
TE-20v	1.200	1.529	1.801	3.243	89.2	1.53	1.616	1.580 ± 0.038	
Cerro Toledo Rhyolite, Indian Point, $J = 0.0005396$, University of Houston									
TE-18a	3.104	8.845	5.440	8.306	90.3	2.62	1.644	1.604 ± 0.029	
TE-18b	2.976	8.878	3.487	6.054	90.5	2.85	1.495	1.455 ± 0.023	
TE-18c	1.058	4.228	3.423	5.887	84.7	2.22	1.576	1.523 ± 0.048	
TE-18d	1.329	2.191	1.863	2.958	86.9	2.37	1.549	1.506 ± 0.080	
TE-18e	8.304	14.512	10.798	18.990	88.1	2.43	1.549	1.474 ± 0.015	
TE-18f	1.688	14.368	8.520	13.456	96.4	3.03	1.546	1.483 ± 0.017	
TE-18g	5.488	7.758	4.941	6.982	82.3	2.83	1.518	1.470 ± 0.029	
TE-18h	9.928	2.242	1.742	2.782	90.4	2.31	1.487	1.411 ± 0.028	
TE-18i	0.740	2.242	1.143	1.759	96.1	3.81	1.480	1.466 ± 0.032	
TE-18j	0.832	4.423	2.635	4.108	94.3	3.00	1.474	1.433 ± 0.030	
TE-18k	0.460	3.572	2.272	3.225	96.2	2.81	1.494	1.458 ± 0.020	
TE-18l	4.432	4.029	2.687	5.323	76.0	2.98	1.518	1.471 ± 0.027	
TE-18m	0.268	3.236	1.727	2.873	97.0	3.33	1.492	1.459 ± 0.043	
TE-18n	0.908	4.066	3.187	4.835	96.4	2.30	1.476	1.438 ± 0.025	
TE-18o	0.512	1.057	1.227	1.857	92.3	1.55	1.478	1.436 ± 0.037	
TE-18p	2.052	2.855	2.118	2.945	83.9	2.43	1.447	1.409 ± 0.023	
TE-18q	0.656	1.084	1.597	2.588	92.7	1.23	1.521	1.480 ± 0.046	
TE-18r	1.728	3.243	1.829	3.259	84.8	2.92	1.425	1.386 ± 0.040	
TE-18s	0.544	3.140	2.387	3.811	95.7	2.38	1.436	1.414 ± 0.029	
TE-18t	2.018	2.874	1.707	3.081	81.1	2.82	1.486	1.427 ± 0.048	
TE-18u	0.344	2.878	2.246	3.538	95.5	2.31	1.512	1.481 ± 0.040	
TE-18v	1.680	1.081	2.590	4.024	82.8	0.78	1.482	1.442 ± 0.038	

(Continued)

SP11. ET AL.

TABLE 3. (Continued)

Sample ID	$^{87}\text{Sr}/^{86}\text{Sr}$	$^{87}\text{Rb}/^{86}\text{Sr}$	$^{87}\text{Rb}/^{86}\text{Sr}$	$^{87}\text{Rb}/^{86}\text{Sr}$	$^{87}\text{Rb}/^{86}\text{Sr}$	$^{87}\text{Rb}/^{86}\text{Sr}$	$^{87}\text{Rb}/^{86}\text{Sr}$	Age (Ma ± 1σ)
	($\pm 1\sigma$)							
Cerro Toledo Rhyolite, Indian Point, $J = 0.0005396$, University of Houston (continued)								
TE-18w	5.488	6.485	2.676	6.198	74.3	3.76	1.500	1.459 ± 0.020
TE-18x	0.496	2.808	1.814	2.811	95.1	3.85	1.520	1.482 ± 0.045
TE-18y	0.720	2.204	3.038	4.856	95.7	1.29	1.533	1.492 ± 0.020
Cerro Toledo Rhyolite, Los Peñas West, $J = 0.0009478$, University of Houston								
TE-25a	0.800	4.784	1.814	3.020	100.3	4.70	1.524	1.569 ± 0.078
TE-25b	0.872	10.988	2.807	4.224	85.5	6.80	1.511	1.249 ± 0.055
TE-25c	4.320	12.828	7.098	11.862	89.5	3.20	1.580	1.534 ± 0.021
TE-25d	1.744	4.427	2.548	4.417	96.7	3.12	1.576	1.587 ± 0.048
TE-25e	0.448	2.839	1.284	2.048	93.9	3.75	1.527	1.508 ± 0.090
TE-25f	1.088	0.899	1.853	3.112	87.0	1.90	1.509	1.521 ± 0.048
TE-25g	2.282	2.483	2.960	2.463	65.6	3.19	1.521	1.502 ± 0.068
TE-25h	0.448	2.094	0.893	1.631	92.3	3.77	1.521	1.561 ± 0.068
TE-25i	0.448	1.088	0.899	1.853	91.2	4.70	1.509	1.521 ± 0.048
TE-25j	0.780	1.401	0.923	1.575	97.6	2.78	1.528	1.561 ± 0.063
TE-25k	2.784	2.474	0.893	8.644	90.8	4.39	1.520	1.506 ± 0.111
TE-25l	0.320	2.300	0.806	1.432	93.6	3.40	1.482	1.510 ± 0.077
TE-25m	1.008	1.988	0.848	3.468	91.8	4.12	1.528	1.512 ± 0.082
TE-25n	0.304	1.347	0.477	2.407	98.4	5.07	1.492	1.480 ± 0.152
TE-25o	0.788	0.000	0.833	1.812	87.3	0.00	1.703	1.736 ± 0.085
TE-25p	2.488	3.058	0.779	1.981	89.2	2.68	1.512	1.548 ± 0.102
TE-25q	0.400	2.569	0.963	1.565	92.8	4.85	1.508	1.508 ± 0.082
Owl Member Bandolite Tuff, Middle Flow Unit, $J = 0.0009478$, University of Houston								
1731UH-1a	10.418	14.823	8.232	16.298	91.3	3.20	1.608	1.646 ± 0.028
1731UH-1b	5.588	9.922	6.848	10.989	85.2	3.08	1.623	1.641 ± 0.021
1731UH-1c	4.800	6.080	3.907	8.047	82.8	2.80	1.707	1.744 ± 0.051
1731UH-1d	11.522	7.588	6.078	11.363	70.8	2.89	1.610	1.681 ± 0.03

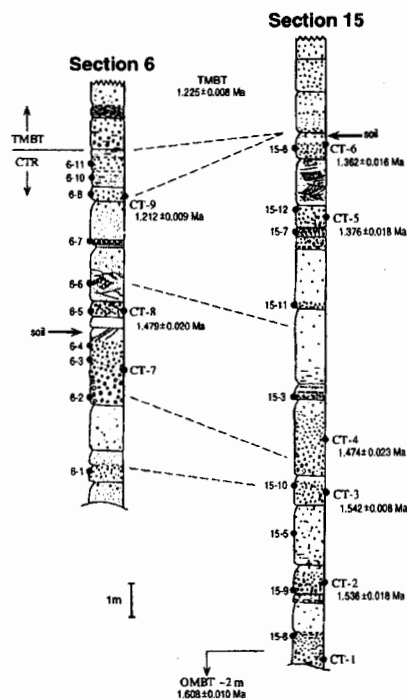


Figure 4. Composite stratigraphic column showing $^{40}\text{Ar}/^{39}\text{Ar}$ dates obtained in this study relative to the stratigraphic position of Cerro Toledo Rhyolite (CTR) tephra samples. Dashed lines between sections indicate correlated units. Arrows indicate soil horizons. Unit numbers as defined by Six (1989). All data from the Australian National University. TMBT is Tshirege Member Bandleier Tuff; OMBT is Otowi Member Bandleier Tuff.

1.37, and 1.21 Ma (Fig. 5). There is a regular progression of decreasing age with higher stratigraphic level, with the exception of the apparent ~150 k.y. gap between samples CT-6 and CT-9 which, as discussed below, may be material loss to erosion. The new dates indicate that the major Cerro Toledo Rhyolite eruptive activity (as recorded by the large pyroclastic pumice units sampled) occurred throughout the ~380 k.y. interval between the Otowi Member and Tshirege Member, and that Cerro Toledo Rhyolite tephra eruptions occurred in distinct pulses ca. 1.54, 1.48, 1.37, and 1.21 Ma (Fig. 5).

The age of sample CT-3 is somewhat problematic. The isochron age of 1.531 ± 0.022 Ma suggests the presence of significant excess argon (Fig. 2), which is not evident for any of the other tephra samples analyzed. On the basis of geochemistry, CT-3 appears to group with samples CT-4, CT-7, and CT-8 (Spell et al., 1996), which are dated here as ca. 1.475 Ma, suggesting a similar age for CT-3. However, neither CT-4 nor CT-8 show signs of excess argon (Fig. 2). Thus, we suggest that the weighted mean age of 1.542 ± 0.008 Ma is preferable due to the very low spread in radiogenic yield among the analyses defining the isochron, but this age is somewhat uncertain.

For samples CT-4 and CT-7, feldspars are dominantly plagioclase and the samples are nearly aphyric, so both plagioclase and sanidine crystals were analyzed. Even though radiogenic yields as high as ~81% were obtained for the plagioclase analyses, the data generally are discordant with coexisting sanidine and with stratigraphic relations, although precision is often poor enough that ages overlap at 2 σ . Sample CT-4 is a good example of this problem because 6 sanidine ages form a coherent group, whereas 10 plagioclase analyses are scattered to both older and, dominantly, younger ages (Table 3). Excess argon could be invoked as an explanation for the older ages because this would affect plagioclase more than sanidine because of the lower K contents of plagioclase. However, the CT-4 sanidine isochron does not indicate the presence of excess argon. All mineral separates analyzed appeared pristine under the binocular microscope, although unrecognized micron-scale alteration cannot be ruled out. Kelley et al. (1994) noted that ultraviolet laser analysis of fractured and/or altered areas in otherwise pristine plagioclase yielded younger ages and suggested that these lowered ages were from alteration products (clays and K-feldspar). A significant correlation between radiogenic yield and age that might be expected from such a mechanism is not seen. However, this might be expected for laser fusion analyses, because the intensity and duration of fusion of individual crystals vary resulting in varying degrees of degassing. The varying amounts of degassing may mask any possible correlation between radiogenic yield and age that may exist. In general, our experience is that total fusion plagioclase ages may not be reliable and should be interpreted with caution (cf. Pringle et al., 1992).

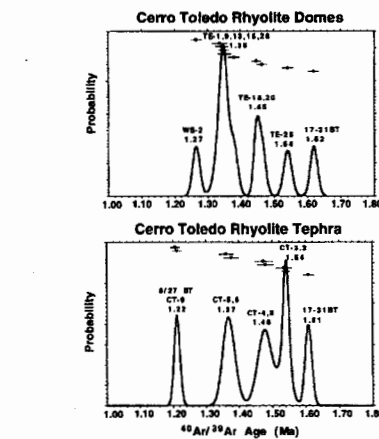


Figure 5. Probability distribution diagram illustrating eruptive periodicity during the interval between the Bandleier tuffs. Sample ages and standard deviations used are preferred $^{40}\text{Ar}/^{39}\text{Ar}$ ages and associated errors from Tables 1 and 2. Modes and samples defining modes are indicated. Cerro Toledo Rhyolite dome samples (upper diagram) analyzed at the University of Houston; tephra samples analyzed at the Australian National University (lower diagram).

which shows that CT-1 must be older than the Otowi Member (1.608 ± 0.010 Ma) and younger than CT-2 (1.536 ± 0.018 Ma) (Fig. 4, Table 1). The observation that CT-9 yields an age identical to that of the overlying Tshirege Member (Table 1) suggests that significant volcanism was occurring immediately prior to the cataclysmic Tshirege Member eruption and collapse of the Valley caldera. These precursor eruptions resulted in deposition of ~1 m of tephra in the sections we studied (Fig. 4), and the geochemistry of CT-9, which is identical to that of the first erupted material of the Tshirege Member (Spell et al., 1996), suggests that these eruptions were rhyolitic. The new $^{40}\text{Ar}/^{39}\text{Ar}$ dates place significant chronological constraints on a magma chamber

recharge event (Six and Garon, 1993) recorded in samples stratigraphically equivalent with units between our samples TT-31 (Otowi Member) and CT-2. Ages of 1.608 ± 0.010 Ma (Otowi Member) and 1.536 ± 0.018 Ma (CT-2) suggest that this event occurred within ~70 k.y. of eruption of the Otowi Member of the Bandleier Tuff and collapse of the Toledo caldera.

Cerro Toledo Rhyolite Domes

Of the nine domes dated in this study, six have been previously dated by the K-Ar method (Zettl et al., 1981; Six et al., 1988; Table 2). The new $^{40}\text{Ar}/^{39}\text{Ar}$ ages are generally consistent with the previously reported ages with the exception that some are slightly older. Cerro Toledo Rhyolite dome samples WS-2, TT-1, TT-20, and TT-25 yield $^{40}\text{Ar}/^{39}\text{Ar}$ ages similar to previous K-Ar ages (Tables 1 and 2) (Zettl et al., 1981; Six et al., 1988). Sample TT-15 from the Turkey Ridge dome as well as TT-26 from Cerro Traqsillar, however, have significantly older $^{40}\text{Ar}/^{39}\text{Ar}$ ages than previous K-Ar ages (Table 2). These older ages probably reflect incomplete degassing of radiogenic argon during K-Ar dating (Webb and McDougall, 1967; McDowell, 1983).

Despite being the most contaminated unit dated in this study, having xenocrysts as old as ca. 105 Ma, Warm Springs dome gave a $^{40}\text{Ar}/^{39}\text{Ar}$ age indistinguishable from the previous K-Ar age (1.265 ± 0.011 Ma vs. 1.25 ± 0.04 Ma, respectively) (Tables 2 and 3). An integrated age (weighted by amount of ^{39}Ar per analysis) of 1.561 ± 0.018 Ma can be calculated from the $^{40}\text{Ar}/^{39}\text{Ar}$ analyses in Table 3. It is common for $^{40}\text{Ar}/^{39}\text{Ar}$ dates to be up to ~10% older (as is the case here for TT-15) than K-Ar dates on sanidine due to incomplete extraction of radiogenic argon during K-Ar analysis (Webb and McDougall, 1967; McDowell, 1983). If the 25 crystals dated from this sample are representative of the crystal population, then the K-Ar age of 1.25 Ma is ~65% younger, which would be unusual. This suggests that the xenocrystic component is over-represented in our analytical data.

The $^{40}\text{Ar}/^{39}\text{Ar}$ age of 1.343 ± 0.015 Ma obtained for Turkey Ridge dome (Table 2) is 8.3% older than the previous K-Ar age of 1.24 ± 0.03 Ma reported by Six et al. (1988). The Unsuared dome gives a $^{40}\text{Ar}/^{39}\text{Ar}$ age of 1.348 ± 0.010 Ma, indistinguishable from the previous K-Ar age of 1.33 ± 0.02 Ma (Table 2). Cerro Traqsillar, sample TT-26, gave a $^{40}\text{Ar}/^{39}\text{Ar}$ age of 1.359 ± 0.012 Ma, which is 7.0% older than the previously reported age of 1.27 ± 0.02 Ma (Table 2).

Sample TT-20, from Los Posos East dome, is, with the exception of tephra sample CT-3 discussed above, the only sample dated in this study

that shows evidence for significant excess ^{40}Ar with an indicated initial $^{40}\text{Ar}/^{39}\text{Ar}$ of 402 ± 33 (Fig. 7). Because most of these analyses are highly radiogenic, the mean and weighted mean ages (calculated assuming an atmospheric initial argon composition) are only $\approx 2\%$ older (contrasting with CT-3 analyses that are less radiogenic, resulting in mean and weighted mean ages $\approx 6\%$ older). Because the TE-20 isochron is defined by a large number of analyses ($n = 20$) with a reasonable spread in radiogenic yield, we take the isochron age as the best estimate of the eruptive age of the Los Posos East dome. The isochron ages of TE-20 (1.446 \pm 0.009 Ma) and CT-3 (1.451 \pm 0.022 Ma) are indistinguishable, suggesting that CT-3 tephra is the Plinian phase of the eruption that produced the Los Posos East dome. However, these two units are distinct geochemically, suggesting that they are unrelated (Spell et al., 1996).

The last Cerro Toledo Rhyolite dome we dated that was previously dated by the K-Ar method is Los Posos West (sample TE-25). Although the $^{40}\text{Ar}/^{39}\text{Ar}$ isochron date of 1.540 \pm 0.012 Ma is within error of the previous 1.50 \pm 0.05 Ma date, it is $\approx 2.7\%$ older and significantly more precise (Table 2).

Cerro Toledo Rhyolite domes dated during this study are within the Toledo embayment with the exception of Warm Springs dome, Cerro Trasquilar, and possibly the Los Posos domes (Fig. 1). There is no apparent regular progression of ages with geographic locality within what remains of the Toledo caldera. Two samples of Sierra de Toledo, a previously undated dome, yield ages of 1.336 \pm 0.018 Ma (TE-9) and 1.379 \pm 0.012 Ma (TE-13), which are 3.2% different and indistinguishable at the 10 confidence level. The Sierra de Toledo dome may be a composite unit produced by multiple eruptions. Note that Turkey Ridge (1.343 \pm 0.015 Ma) and the Sierra de Toledo dome form a continuous morphological feature and thus may represent a single eruptive event between ≈ 1.34 and 1.38 Ma.

The most obvious aspect of the $^{40}\text{Ar}/^{39}\text{Ar}$ dates on Cerro Toledo Rhyolite domes is the fact that five of the nine samples dated fall in an interval between the dates on the two Sierra de Toledo samples TE-9 and TE-13. This is also an interval of time during which two of the Cerro Toledo Rhyolite tephra samples (CT-5, CT-6) were erupted (Fig. 2, Table 1). The previously undated Indian Point dome gave a $^{40}\text{Ar}/^{39}\text{Ar}$ age of 1.463 \pm 0.011 Ma. As with Cerro Toledo Rhyolite tephra samples, the domes dated were erupted during discrete periods, separated by longer quiescent intervals. Eruptions occurred at 1.54, 1.45, 1.38–1.34, and 1.27 Ma. Quiescent intervals of 70–80 k.y. separate these volcanic periods.

Correlations Between Cerro Toledo Rhyolite Tephra and Domes

Initial speculations on correlations between Cerro Toledo Rhyolite tephra and domes were made by Heiken et al. (1986), who suggested that the Los Posos (East Los Posos in particular) domes of the Cerro Toledo domes correspond to tephra units that include our samples CT-1, CT-2, CT-3, CT-4, and CT-7 in stratigraphic levels 5 through 23 (Table 1). Heiken et al. (1986) also indicated that stratigraphic levels 26 through 41 (Table 1) (CT-8, CT-5, CT-6, and CT-9) correlate with Pinnacle Peak, which was not dated in this study.

Six et al. (1988) discussed correlations between Cerro Toledo Rhyolite tephra and domes based on the more detailed geochemistry and geochronology available at that time. They suggested that the Los Posos domes (Fig. 1) with K-Ar ages of 1.47–1.50 Ma (Heiken et al., 1986) correlate with tephra units corresponding to our samples CT-1, CT-4, and CT-7, which are dated here as 1.47 to 1.54 Ma (Table 1). Stratigraphic units, below which our sample CT-8 lies, were suggested to correlate with the Turkey Ridge domes (dated as 1.24 \pm 0.03 Ma by Heiken et al., 1986). The Southwest Rhyolite dome, Pinnacle Peak, Warm Springs dome, and Cerro Trasquilar were suggested to correlate with tephra units corresponding to our samples CT-6 through CT-9 (Six et al., 1988).

The $^{40}\text{Ar}/^{39}\text{Ar}$ ages reported here (Tables 1 and 2) allow these correlations to be tested. Both Cerro Toledo Rhyolite tephra and dome samples record periodic volcanic activity and have similar timing for these eruptive periods. Eruptive activity is recorded in Cerro Toledo Rhyolite tephra at 1.54, 1.45, 1.37, and 1.21 Ma. A similar timing of eruptive episodes is defined by the Cerro Toledo Rhyolite dome samples dated in this study as 1.54, 1.45, 1.38–1.34, and 1.27 Ma (Fig. 5).

Tephra samples CT-2 and CT-3 (1.536 \pm 0.018 and 1.542 \pm 0.008 Ma, respectively) from near the base of the section yield ages identical to those obtained on Los Posos West dome sample TE-25 (1.540 \pm 0.012 Ma). This result confirms the suggestions of Heiken et al. (1986) and Six et al. (1988) that CT-2 and CT-3 correlate with the Los Posos West dome, but shows that Los Posos East (see below) does not correlate to these stratigraphic levels in the tephra and also shows that CT-4 and CT-7 are not correlative with Los Posos West (Fig. 5).

Further upsection, tephra samples CT-4 and CT-8 (1.474 \pm 0.023 and 1.479 \pm 0.020 Ma, respectively) correlate with the Indian Point and Los Posos East domes samples TE-18 and TE-20 (1.463 \pm 0.011 and 1.446 \pm 0.009 Ma, respectively), although there is a suggestion that

Los Posos East may be slightly younger than these. Cerro Toledo Rhyolite tephra samples Heiken et al. (1986) and Six et al. (1988) suggested the correlation between CT-4 and Los Posos East which our $^{40}\text{Ar}/^{39}\text{Ar}$ dates confirm. Six et al. (1988) correlated a section of Cerro Toledo Rhyolite tephra with the Turkey Ridge dome. Our CT-8 sample lies below this. The 1.479 Ma $^{40}\text{Ar}/^{39}\text{Ar}$ age for CT-8 and the 1.343 Ma $^{40}\text{Ar}/^{39}\text{Ar}$ date on TE-15, from Turkey Ridge, do not support this correlation.

Tephra samples CT-5 and CT-6 (1.376 \pm 0.018 and 1.362 \pm 0.016, respectively) correlate temporally with a large group of samples from Sierra de Toledo, Cerro Trasquilar, Unnamed dome, and Turkey Ridge, samples TE-13 (1.379 \pm 0.012 Ma), TE-26 (1.351 \pm 0.015 Ma), TE-1 (1.348 \pm 0.010 Ma), TE-15 (1.343 \pm 0.015 Ma), and TE-9 (1.336 \pm 0.018 Ma). Six et al. (1988) suggested the correlation between CT-6 and the Warm Springs and Cerro Trasquilar domes, which is supported by our data.

There is no correlative tephra for the Warm Springs dome (WS-2; 1.265 \pm 0.011 Ma). Six et al. (1988) indicated a correlation between tephra corresponding to CT-6 and CT-9 with the Warm Springs dome. Our data show that CT-6 is significantly older and CT-9 significantly younger than the Warm Springs dome (Tables 1 and 2). There is no Plinian pumice fall unit within the Cerro Toledo Rhyolite tephra sections we sampled—stratigraphically between CT-6 and CT-9—that might represent the initial phase of the eruption producing the Warm Springs dome.

At the top of the Cerro Toledo Rhyolite stratigraphic section, tephra sample CT-9 (1.212 \pm 0.009 Ma) does not correlate with any domes dated in this study, however, it has an age indistinguishable from that of the Tibirige Member (1.225 \pm 0.008 Ma). This is consistent with the geochemistry of CT-9, which is indistinguishable from the overlying Tibirige Member Plinian pumice (Spell et al., 1996).

SUMMARY

The Cerro Toledo Rhyolites record volcanism during the ≈ 80 k.y. interval between two caldera-forming eruptions: the Tibirige and Otowi members of the Banderler Tuff in the Jemez Volcanic Field. They contain important information about the evolution of this large crustal silicic magma system during the transition from and to caldera collapse events; this study provides the good chronological control which is essential for interpreting such data.

$^{40}\text{Ar}/^{39}\text{Ar}$ dating of nine major pumice fall units within the Cerro Toledo Rhyolite tephra, which may record the inception of significant dome extrusion events within the Toledo caldera,

yields a detailed chronology of eruptive activity; seven of these units are reliable and stratigraphically consistent ages. With a few exceptions, reliable isochron ages were obtained from multiple laser fusions of individual phenocrysts. For some sparsely porphyritic samples in which the dominant phenocryst is plagioclase, this phase was analyzed. Plagioclase dates were generally of poor precision, discordant with co-existing sanidine, and inconsistent with stratigraphic constraints. The dates obtained suggest that Cerro Toledo Rhyolite Plinian pumice fall eruptions occurred throughout the interval between the Banderler tuffs (ca. 1.61–1.23 Ma), but that sequences of these eruptions occurred in pulses at ca. 1.54, 1.48, 1.37, and 1.22 Ma.

$^{40}\text{Ar}/^{39}\text{Ar}$ dates indicate that Cerro Toledo Rhyolite tephra were produced at 1.54, 1.45, 1.38–1.34, and 1.27 Ma, and show that many can be correlated chronologically with the tephra sequence. The oldest and youngest Cerro Toledo Rhyolite tephra are indistinguishable in age from the Otowi Member and Tibirige Member, respectively, and thus their geochemistry may provide insight into the final products of the Otowi Member magma chamber and the earliest phases of the Tibirige Member magma chamber.

The eruptive chronology provided by this study, when combined with geochemical and isochron data (Six and Gorton, 1993; Spell et al., 1996) should significantly enhance our understanding of the evolution of the Banderler silicic magma system. For example, evidence for a magma chamber recharge event recorded in Cerro Toledo Rhyolite tephra immediately after the Otowi Member (Six and Gorton, 1993), combined with stratigraphic and age constraints, indicate that this occurred within ≈ 70 k.y. of caldera collapse.

ACKNOWLEDGMENTS

The Black Land and Cattle Company allowed us access to their land for sample collection. We thank P. Kyle for collaboration on Jemez Volcanic Field studies and J. Six for sharing his knowledge of stratigraphic relationships in the Cerro Toledo Rhyolite tephra. J. Wolf supplied samples from the Banderler Tuff. J. Mya and S. Paxton assisted with mineral separations and R. Maier provided technical support during the laboratory calibration and K-Ar analyses of our Fish Canyon Tuff standard, separate 92-176 at the Australian Nuclear Energy Research Institute of Nuclear Science and Engineering and

the Australian Nuclear Science and Technology Organization and by the Department of Energy and the Nuclear Science Center at Texas A&M University. Establishment of the University of Houston Thermochemical Laboratory was funded by National Science Foundation grant EAR-9219005 to P. Copeland. An early version of the manuscript benefited from comments by P. Kyle, J. Six, and J. Wolff. Reviews by J. Gardner and W. McIntosh helped improve and refine the manuscript.

REFERENCES CITED

Baker, R. A., Smith, R. L., and Foy, C. S., 1969. Stratigraphic correlation of volcanic units in the Jemez Mountains, New Mexico. U.S. Geological Survey Bulletin 1277, p. 1–19.

Balcer, D. L., 1983. The geology and geochronology of the Tibirige Member of the Banderler Tuff, Jemez Mountains, New Mexico. U.S. Geological Survey Bulletin 1379, p. 1–134.

Bogert, P. V., 1995. $^{40}\text{Ar}/^{39}\text{Ar}$ ages of sanidine phenocrysts from the Tibirige Member of the Banderler Tuff, Jemez Mountains, New Mexico. M.S. thesis, Colorado State University, Fort Collins, Colorado, 118 p.

Calvin, C. J., Smith, R. L., Johnson, H. H., Foy, C. W., Gendron, J. D., and Sarna, J., 1986. The Fish Canyon Tuff: a potential standard for the $^{40}\text{Ar}/^{39}\text{Ar}$ and electron-impact methods. *Earth and Planetary Science Letters*, 84, p. 1–17.

Chambers, J. M., and Delaney, D. J., 1993. Two weeks of large volume eruptive activity: eruption sequence of phenocrystic and glass from the Bandy Tuff, Long Valley Caldera, California. *Journal of Volcanology and Geothermal Research*, 51, p. 105–115.

Delaney, D. J., and Lander, M. A., 1971. $^{40}\text{Ar}/^{39}\text{Ar}$ as a measure of K-Ar ages. A comparison between the conventional technique. *Earth and Planetary Science Letters*, 11, p. 309–308.

Dixon, G. R., Hollister, A. C., Robinson, C. A., and Hall, C. M., 1964. Isotopic changes in the production zone, crystallization zone, and residence time of pre-eruptive silicic magma. *Long Valley, California. Earth and Planetary Science Letters*, 1, p. 125–137.

Dixon, A. L., and Pelt, R., 1996. Single-crystal $^{40}\text{Ar}/^{39}\text{Ar}$ as a test of the Open-system Fractionation, unmixing, and/or loss of argon. *Earth and Planetary Science Letters*, 137, p. 811–819.

Drexler, R. B., and Delaney, D. J., 1984. Geochronology of a rhyolite flow: product of the age of the Bandy Tuff, Long Valley Caldera, California. *Journal of Volcanology and Geothermal Research*, 3, p. 191–193.

Drexler, R. B., Delaney, D. J., Smith, R. L., and Bailey, R. A., 1984. Plagioclase, phenocryst, and glass: age and zoning of rhyolite and associated rocks of the Valle Grande, New Mexico. *Geological Society of America Bulletin*, 95, p. 711–718.

Gardner, J. H., and Goff, F., 1984. Plinian eruption dates from the Jemez Volcanic Field, New Mexico, with special reference to the Bandy Tuff. *New Mexico Geological Society*, 35, p. 71–78.

Gardner, J. H., Goff, F., and Hagan, R. L., 1986. Stratigraphic correlation and dating of rhyolite flows in the Jemez Volcanic Field, New Mexico. *Journal of Volcanology and Geothermal Research*, 31, p. 161–178.

Griggs, R. L., 1964. Geology and ground water of the Los Posos area, New Mexico. U.S. Geological Survey Water-Supply Paper 1753, 80 p.

Halliday, A. N., Mahood, G. A., Holdren, P., Metz, J. M., Chatterjee, T. J., and Jambon, J. P., 1996. Evidence for magma chamber recharge: the rhyolite eruption in the Long Valley magmatic system. The eruption record in pre-eruptive levels of Glass Mountain, Long Valley Caldera and Eastwoodhorn, Sierra Nevada. *New Mexico Journal of Geology*, 26, p. 774–790.

Heiken, G., Goff, F., Sims, T., Tammey, G., Hargill, M., Garcia, S., and Hagan, R., 1986. Borehole, seismic, activity. *Sierra Nevada and Eastwoodhorn, Sierra Nevada. New Mexico Journal of Geology*, 26, p. 179–183.

Hildreth, W., 1981. Craters in silicic eruption chambers: Implications for subsurface evolution. *Journal of Geophysical Research*, 86, p. 10,351–10,372.

Hildreth, W., and Haxel, R. S., 1985. The geochronology of an eruption by removal of fresh base-concentrated crust. *Journal of Petrology*, 26, p. 209–240.

Hornok, A. J., and Delaney, D. J., 1981. $^{40}\text{Ar}/^{39}\text{Ar}$ and K-Ar dating of the Tibirige and Fish Canyon tuffs, California, and the Bandy Tuff, Idaho. *Journal of Geophysical Research*, 86, p. 10,373–10,381.

Lark, D. A., and Delaney, D. J., 1984. $^{40}\text{Ar}/^{39}\text{Ar}$ age constraints for

the Bandy Tuff, Idaho, and the Westwood, Oregon, plagioclase standard. *Journal of Geophysical Research*, 89, p. 2923–2934.

Lark, D. A., Hildreth, W., Foy, C. W., and Collins, G. T., 1981. Plinian eruption and facies-tuff chronology of Cerro Toledo Rhyolite tephra in the Jemez Mountains, New Mexico. U.S. Geological Survey Professional Paper 1190-2, p. 27–41.

Lindley, J. P., and Foy, C. W., and Foy, C. P., 1962. High vacuum $^{40}\text{Ar}/^{39}\text{Ar}$ investigations using an electron beam probe as a source of argon. *Geochimica et Cosmochimica Acta*, 26, p. 1511–1525.

Moore, J. F., 1988. The first Member of the Banderler Tuff: a study of the tephrology, geochronology, and geochemistry of an explosive silicic eruption. *Sierra Nevada, New Mexico*. M.S. thesis, University of Texas, Austin, 163 p.

Phillips, P. W., 1981. The effect of total chlorine on isochron methods. *Journal of Geophysical Research*, 86, p. 8011–8015.

Spiegel, F. W., 1983. K-Ar dates: Interpretation of radiogenic argon from alkali feldspar. *Journal of Geophysical Research*, 88, p. 119–123.

Spiegel, F. W., McWilliam, M., Chatterjee, R. J., Stephens, M. A., and Wilson, C. B., 1992. $^{40}\text{Ar}/^{39}\text{Ar}$ dating of Quaternary feldspar. *Examples from the Taupo Volcanic Zone, New Zealand*. *Geology*, 20, p. 333–334.

Strom, C. L., Gardner, J. H., and Foy, C. W., 1996. New evidence for age of the eruption sequence in the Valle Grande, New Mexico. *Geology*, 24, p. 7–10.

Sterner, S., Goff, F., Delaney, D. J., Wofford, J. V., and Kyle, W. M., 1986. Felsophic rhyolite volcanism in the Jemez Mountains, New Mexico, during emplacement and late-stage magmatic structure. *Journal of Geophysical Research*, 91, p. 1779–1788.

Smith, R. L., 1990. $^{40}\text{Ar}/^{39}\text{Ar}$ dating. *Geological Society of America Special Paper* 180, p. 3–17.

Smith, R. L., and Bandy, R. A., 1984. Rhyolite calderas. *Geological Society of America Memoir* 174, p. 413–460.

Smith, R. L., Bandy, R. A., and Robinson, C. A., 1978. Geologic map of the Jemez Mountains, New Mexico. U.S. Geological Survey Miscellaneous Geologic Map 1-515, 1:250,000.

Spiegel, F. W., and Foy, C. W., 1982. $^{40}\text{Ar}/^{39}\text{Ar}$ geochronology of plagioclase, sanidine, and glass. *Journal of Geophysical Research*, 87, p. 10,799–10,796.

Spiegel, F. W., and Foy, C. W., 1989. Progression of Valle Grande Member rhyolite, Valle Grande, New Mexico: Implications for a caldera of the Jemez Mountains magmatic system. *Journal of Geophysical Research*, 94, p. 10,799–10,796.

Spiegel, F. W., and Foy, C. W., 1993. $^{40}\text{Ar}/^{39}\text{Ar}$ dating of the Banderler Tuff and Los Posos Rhyolite: Temporal correlation of an explosive eruption. *Journal of Volcanology and Geothermal Research*, 51, p. 175–181.

Spiegel, F. W., Foy, C. W., and Delaney, D. J., 1990. Geochronology and geochemistry of the Cerro Toledo Rhyolite, New Mexico. *Geological Society of America Bulletin*, 101, p. 121–130.

Spiegel, F. W., and Hagan, R. L., 1982. $^{40}\text{Ar}/^{39}\text{Ar}$ geochronology of plagioclase, sanidine, and glass. *Journal of Geophysical Research*, 87, p. 10,799–10,796.

Spiegel, F. W., and Foy, C. W., 1989. Progression of Valle Grande Member rhyolite, Valle Grande, New Mexico: Implications for a caldera of the Jemez Mountains magmatic system. *Journal of Geophysical Research*, 94, p. 10,799–10,796.

Spiegel, F. W., and Foy, C. W., 1993. $^{40}\text{Ar}/^{39}\text{Ar}$ dating of the Banderler Tuff and Los Posos Rhyolite: Temporal correlation of an explosive eruption. *Journal of Volcanology and Geothermal Research*, 51, p. 175–181.

Spiegel, F. W., Foy, C. W., and Delaney, D. J., 1990. Geochronology and geochemistry of the Cerro Toledo Rhyolite, New Mexico. *Geological Society of America Bulletin*, 101, p. 121–130.

Spiegel, F. W., and Hagan, R. L., 1982. $^{40}\text{Ar}/^{39}\text{Ar}$ geochronology of plagioclase, sanidine, and glass. *Journal of Geophysical Research*, 87, p. 10,799–10,796.

Spiegel, F. W., and Foy, C. W., 1989. Progression of Valle Grande Member rhyolite, Valle Grande, New Mexico: Implications for a caldera of the Jemez Mountains magmatic system. *Journal of Geophysical Research*, 94, p. 10,799–10,796.

Spiegel, F. W., and Foy, C. W., 1993. $^{40}\text{Ar}/^{39}\text{Ar}$ dating of the Banderler Tuff and Los Posos Rhyolite: Temporal correlation of an explosive eruption. *Journal of Volcanology and Geothermal Research*, 51, p. 175–181.

Spiegel, F. W., Foy, C. W., and Delaney, D. J., 1990. Geochronology and geochemistry of the Cerro Toledo Rhyolite, New Mexico. *Geological Society of America Bulletin*, 101, p. 121–130.

Spiegel, F. W., and Hagan, R. L., 1982. $^{40}\text{Ar}/^{39}\text{Ar}$ geochronology of plagioclase, sanidine, and glass. *Journal of Geophysical Research*, 87, p. 10,799–10,796.

Spiegel, F. W., and Foy, C. W., 1989. Progression of Valle Grande Member rhyolite, Valle Grande, New Mexico: Implications for a caldera of the Jemez Mountains magmatic system. *Journal of Geophysical Research*, 94, p. 10,799–10,796.

Spiegel, F. W., and Foy, C. W., 1993. $^{40}\text{Ar}/^{39}\text{Ar}$ dating of the Banderler Tuff and Los Posos Rhyolite: Temporal correlation of an explosive eruption. *Journal of Volcanology and Geothermal Research*, 51, p. 175–181.

Spiegel, F. W., Foy, C. W., and Delaney, D. J., 1990. Geochronology and geochemistry of the Cerro Toledo Rhyolite, New Mexico. *Geological Society of America Bulletin*, 101, p. 121–130.

Spiegel, F. W., and Hagan, R. L., 1982. $^{40}\text{Ar}/^{39}\text{Ar}$ geochronology of plagioclase, sanidine, and glass. *Journal of Geophysical Research*, 87, p. 10,799–10,796.

Spiegel, F. W., and Foy, C. W., 1989. Progression of Valle Grande Member rhyolite, Valle Grande, New Mexico: Implications for a caldera of the Jemez Mountains magmatic system. *Journal of Geophysical Research*, 94, p. 10,799–10,796.

Spiegel, F. W., and Foy, C. W., 1993. $^{40}\text{Ar}/^{39}\text{Ar}$ dating of the Banderler Tuff and Los Posos Rhyolite: Temporal correlation of an explosive eruption. *Journal of Volcanology and Geothermal Research*, 51, p. 175–181.

Spiegel, F. W., Foy, C. W., and Delaney, D. J., 1990. Geochronology and geochemistry of the Cerro Toledo Rhyolite, New Mexico. *Geological Society of America Bulletin*, 101, p. 121–130.

Spiegel, F. W., and Hagan, R. L., 1982. $^{40}\text{Ar}/^{39}\text{Ar}$ geochronology of plagioclase, sanidine, and glass. *Journal of Geophysical Research*, 87, p. 10,799–10,796.

Spiegel, F. W., and Foy, C. W., 1989. Progression of Valle Grande Member rhyolite, Valle Grande, New Mexico: Implications for a caldera of the Jemez Mountains magmatic system. *Journal of Geophysical Research*, 94, p. 10,799–10,796.

Spiegel, F. W., and Foy, C. W., 1993. $^{40}\text{Ar}/^{39}\text{Ar}$ dating of the Banderler Tuff and Los Posos Rhyolite: Temporal correlation of an explosive eruption. *Journal of Volcanology and Geothermal Research*, 51, p. 175–181.

Spiegel, F. W., Foy, C. W., and Delaney, D. J., 1990. Geochronology and geochemistry of the Cerro Toledo Rhyolite, New Mexico. *Geological Society of America Bulletin*, 101, p. 121–130.

Spiegel, F. W., and Hagan, R. L., 1982. $^{40}\text{Ar}/^{39}\text{Ar}$ geochronology of plagioclase, sanidine, and glass. *Journal of Geophysical Research*, 87, p. 10,799–10,796.

Spiegel, F. W., and Foy, C. W., 1989. Progression of Valle Grande Member rhyolite, Valle Grande, New Mexico: Implications for a caldera of the Jemez Mountains magmatic system. *Journal of Geophysical Research*, 94, p. 10,799–10,796.

Spiegel, F. W., and Foy, C. W., 1993. $^{40}\text{Ar}/^{39}\text{Ar}$ dating of the Banderler Tuff and Los Posos Rhyolite: Temporal correlation of an explosive eruption. *Journal of Volcanology and Geothermal Research*, 51, p. 175–181.

Spiegel, F. W., Foy, C. W., and Delaney, D. J., 1990. Geochronology and geochemistry of the Cerro Toledo Rhyolite, New Mexico. *Geological Society of America Bulletin*, 101, p. 121–130.

Spiegel, F. W., and Hagan, R. L., 1982. $^{40}\text{Ar}/^{39}\text{Ar}$ geochronology of plagioclase, sanidine, and glass. *Journal of Geophysical Research*, 87, p. 10,799–10,796.

Spiegel, F. W., and Foy, C. W., 1989. Progression of Valle Grande Member rhyolite, Valle Grande, New Mexico: Implications for a caldera of the Jemez Mountains magmatic system. *Journal of Geophysical Research*, 94, p. 10,799–10,796.

Spiegel, F. W., and Foy, C. W., 1993. $^{40}\text{Ar}/^{39}\text{Ar}$ dating of the Banderler Tuff and Los Posos Rhyolite: Temporal correlation of an explosive eruption. *Journal of Volcanology and Geothermal Research*, 51, p. 175–181.

Spiegel, F. W., Foy, C. W., and Delaney, D. J., 1990. Geochronology and geochemistry of the Cerro Toledo Rhyolite, New Mexico. *Geological Society of America Bulletin*, 101, p. 121–130.

Spiegel, F. W., and Hagan, R. L., 1982. $^{40}\text{Ar}/^{39}\text{Ar}$ geochronology of plagioclase, sanidine, and glass. *Journal of Geophysical Research*, 87, p. 10,799–10,796.

Spiegel, F. W., and Foy, C. W., 1989. Progression of Valle Grande Member rhyolite, Valle Grande, New Mexico: Implications for a caldera of the Jemez Mountains magmatic system. *Journal of Geophysical Research*, 94, p. 10,799–10,796.

Spiegel, F. W., and Foy, C. W., 1993. $^{40}\text{Ar}/^{39}\text{Ar}$ dating of the Banderler Tuff and Los Posos Rhyolite: Temporal correlation of an explosive eruption. *Journal of Volcanology and Geothermal Research*, 51, p. 175–181.

Spiegel, F. W., Foy, C. W., and Delaney, D. J., 1990. Geochronology and geochemistry of the Cerro Toledo Rhyolite, New Mexico. *Geological Society of America Bulletin*, 101, p. 121–130.

Spiegel, F. W., and Hagan, R. L., 1982. $^{40}\text{Ar}/^{39}\text{Ar}$ geochronology of plagioclase, sanidine, and glass. *Journal of Geophysical Research*, 87, p. 10,799–10,796.

Spiegel, F. W., and Foy, C. W., 1989. Progression of Valle Grande Member rhyolite, Valle Grande, New Mexico: Implications for a caldera of the Jemez Mountains magmatic system. *Journal of Geophysical Research*, 94, p. 10,799–10,796.

Spiegel, F. W., and Foy, C. W., 1993. $^{40}\text{Ar}/^{39}\text{Ar}$ dating of the Banderler Tuff and Los Posos Rhyolite: Temporal correlation of an explosive eruption. *Journal of Volcanology and Geothermal Research*, 51, p. 175–181.

Spiegel, F. W., Foy, C. W., and Delaney, D. J., 1990. Geochronology and geochemistry of the Cerro Toledo Rhyolite, New Mexico. *Geological Society of America Bulletin*, 101, p. 121–130.

Spiegel, F. W., and Hagan, R. L., 1982. $^{40}\text{Ar}/^{39}\text{Ar}$ geochronology of plagioclase, sanidine, and glass. *Journal of Geophysical Research*, 87, p. 10,799–10,796.

Spiegel, F. W., and Foy, C. W., 1989. Progression of Valle Grande Member rhyolite, Valle Grande, New Mexico: Implications for a caldera of the Jemez Mountains magmatic system. *Journal of Geophysical Research*, 94, p. 10,799–10,796.

Spiegel, F. W., and Foy, C. W., 1993. $^{40}\text{Ar}/^{39}\text{Ar}$ dating of the Banderler Tuff and Los Posos Rhyolite: Temporal correlation of an explosive eruption. *Journal of Volcanology and Geothermal Research*, 51, p. 175–181.

Spiegel, F. W., Foy, C. W., and Delaney, D. J., 1990. Geochronology and geochemistry of the Cerro Toledo Rhyolite, New Mexico. *Geological Society of America Bulletin*, 101, p. 121–130.

Spiegel, F. W., and Hagan, R. L., 1982. $^{40}\text{Ar}/^{39}\text{Ar}$ geochronology of plagioclase, sanidine, and glass. *Journal of Geophysical Research*, 87, p. 10,799–10,796.

Spiegel, F. W., and Foy, C. W., 1989. Progression of Valle Grande Member rhyolite, Valle Grande, New Mexico: Implications for a caldera of the Jemez Mountains magmatic system. *Journal of Geophysical Research*, 94, p. 10,799–10,796.

Spiegel, F. W., and Foy, C. W., 1993. $^{40}\text{Ar}/^{39}\text{Ar}$ dating of the Banderler Tuff and Los Posos Rhyolite: Temporal correlation of an explosive eruption. *Journal of Volcanology and Geothermal Research*, 51, p. 175–181.

Spiegel, F. W., Foy, C. W., and Delaney, D. J., 1990. Geochronology and geochemistry of the Cerro Toledo Rhyolite, New Mexico. *Geological Society of America Bulletin*, 101, p. 121–130.

Spiegel, F. W., and Hagan, R. L., 1982. $^{40}\text{Ar}/^{39}\text{Ar}$ geochronology of plagioclase, sanidine, and glass. *Journal of Geophysical Research*, 87, p. 10,799–10,796.

Spiegel, F. W., and Foy, C. W., 1989. Progression of Valle Grande Member rhyolite, Valle Grande, New Mexico: Implications for a caldera of the Jemez Mountains magmatic system. *Journal of Geophysical Research*, 94, p. 10,799–10,796.

Spiegel, F. W., and Foy, C. W., 1993. $^{40}\text{Ar}/^{39}\text{Ar}$ dating of the Banderler Tuff and Los Posos Rhyolite: Temporal correlation of an explosive eruption. *Journal of Volcanology and Geothermal Research*, 51, p. 175–181.

Spiegel, F. W., Foy, C. W., and Delaney, D. J., 1990. Geochronology and geochemistry of the Cerro Toledo Rhyolite, New Mexico. *Geological Society of America Bulletin*, 101, p. 121–130.

Spiegel, F. W., and Hagan, R. L., 1982. $^{40}\text{Ar}/^{39}\text{Ar}$ geochronology of plagioclase, sanidine, and glass. *Journal of Geophysical Research*, 87, p. 10,799–10,796.

Spiegel, F. W., and Foy, C. W., 1989. Progression of Valle Grande Member rhyolite, Valle Grande, New Mexico: Implications for a caldera of the Jemez Mountains magmatic system. *Journal of Geophysical Research*, 94, p. 10,799–10,796.

Spiegel, F. W., and Foy, C. W., 1993. $^{40}\text{Ar}/^{39}\text{Ar}$ dating of the Banderler Tuff and Los Posos Rhyolite: Temporal correlation of an explosive eruption. *Journal of Volcanology and Geothermal Research*, 51, p. 175–181.

Spiegel, F. W., Foy, C. W., and Delaney, D. J., 1990. Geochronology and geochemistry of the Cerro Toledo Rhyolite, New Mexico. *Geological Society of America Bulletin*, 101, p. 121–130.

Spiegel, F. W., and Hagan, R. L., 1982. $^{40}\text{Ar}/^{39}\text{Ar}$ geochronology of plagioclase, sanidine, and glass. *Journal of Geophysical Research*, 87, p. 10,799–10,796.

Spiegel, F. W., and Foy, C. W., 1989. Progression of Valle Grande Member rhyolite, Valle Grande, New Mexico: Implications for a caldera of the Jemez Mountains magmatic system. *Journal of Geophysical Research*, 94, p. 10,799–10,796.

Spiegel, F. W., and Foy, C. W., 1993. $^{40}\text{Ar}/^{39}\text{Ar}$ dating of the Banderler Tuff